NASA CR-114859

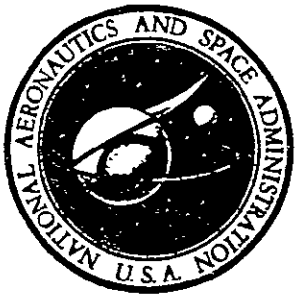

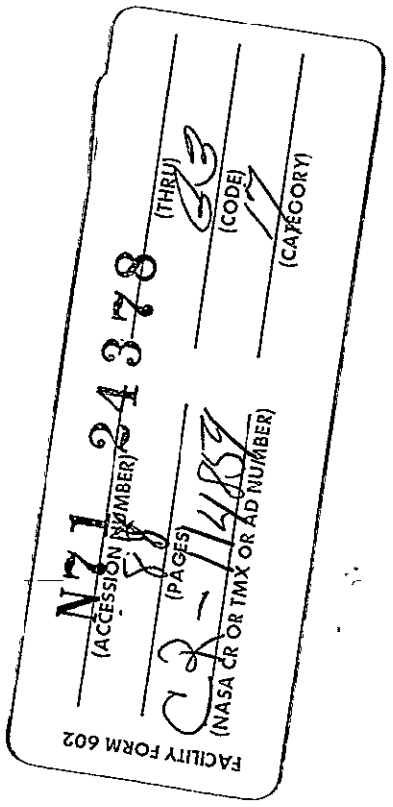

CRACK GROWTH OF 5Al-2.5Sn TITANIUM IN HYDROGEN

By
W. D. Bixler And W. L. Engstrom

Prepared for

NATIONAL AERONAUTICS AND SPACE ADMINISTRATION

Contract NAS 9-11435

THE BOEING COMPANY

Requests for copies of this report should be referred to

National Aeronautics and Space Administration
Office of Scientific and Technical Information
Attention: AFSS-A
Washington, D.C. 20546

Final Report

CRACK GROWTH OF 5Al-2.5Sn TITANIUM IN HYDROGEN

By

W. D. Bixler and W. L. Engstrom

Prepared for

NATIONAL AERONAUTICS AND SPACE ADMINISTRATION

March 1971

Contract NAS 9-11435

Technical Management

NASA Manned Spacecraft Center
Houston, Texas

S. V. Glorioso

Aerospace Group

THE BOEING COMPANY

Seattle, Washington

CRACK GROWTH OF 5Al-2.5Sn TITANIUM IN HYDROGEN

By

W. D. Bixler and W. L. Engstrom

ABSTRACT

Fracture and subcritical flaw growth characteristics were experimentally determined for 5Al-2.5Sn (ELI) titanium in an environment of low pressure, high purity gaseous hydrogen. The actual material tested consisted of forging parent metal and electron beam (EB) welded forging and plate which were tested in the weld heat affected zone (HAZ) and weld centerline ($\mathbb{C}$), respectively. Static fracture, sustained load and cyclic load tests were conducted using precracked surface flawed specimens. Specimens with simulated lack-of-penetration weld defects were used to investigate the effects of very long, deep flaws. Specimen thicknesses, welding procedures and environments were selected to simulate those of the Apollo Service Module/Electrical Power System (SM/EPS) cryo-hydrogen tank. For this tank, the failure mode was found to be leakage at proof and operating stress levels. Environmentally induced flaw growth was observed at stresses exceeding the proof stress at 70°F & -200°F, but not at -423°F. For flaw sizes that might go undetected during nondestructive inspection (NDI), no flaw growth would be expected when loaded to the maximum design operating stress (σ_{MDOP}) for flaw depths up to approximately 90 percent of the thickness. Time dependent growth at σ_{MDOP} was observed for flaws that were very long (1.5"—►3.0"). In addition, cyclic flaw growth rates at stress levels and stress ratios applicable to the SM/EPS cryo-hydrogen tank are essentially zero.

KEY WORDS

5Al-2.5Sn(ELI) titanium

Low Pressure, high purity gaseous hydrogen

Fracture characteristics

SUMMARY

The experimental work described herein was undertaken to investigate the fracture and flaw growth characteristics of forging and EB welded 5Al-2.5Sn(ELI) titanium, primarily in an environment of low pressure, high purity gaseous hydrogen. The primary objective was to determine the failure mode and sustained load growth characteristics applicable to the SM/EPS cryo-hydrogen tank.

The program was primarily conducted using precracked surface flawed specimens. Specimens with flaws simulating lack-of-penetration weld defects were also used to determine the fracture characteristics of very long, deep flaws. Tank fabrication processes, thicknesses and service conditions were simulated in this program. Static, sustain and cyclic loaded specimens were tested with flaws located in the base metal, in weld nugget centerline and in weld heat affected zone.

Flaw growth tests were conducted in 300 psia gaseous hydrogen at temperatures of 70°F, -200°F and -423°F. Static fracture tests and some cyclic load tests were conducted in air at 70°F, in air/gaseous nitrogen at -200°F, and in liquid hydrogen at -423°F. Welded specimens (which were tested in the as-welded condition) were nominally 0.061" thick and base metal specimens were nominally 0.044" thick.

The following observations and conclusions were made from the study:

1. Failure mode of the SM/EPS cryo-hydrogen tank is leakage at both proof and operating stress levels for temperatures ranging from 70°F to -423°F for flaw lengths less than 3.0".

2. Environmentally induced flaw growth was observed in testing 5Al-2.5Sn(ELI) titanium in low pressure, high purity gaseous hydrogen at 70°F and -200°F, but none was observed at -423°F. The time dependent flaw growth that was observed, occurred at stresses exceeding the proof stress. No flaw growth

would be expected when loaded to σ_{MDOP} for flaw depths up to approximately 90 percent of the thickness. These observations were based on flaws that were less than 0.5 inches long. As the flaw length increased to 1.5 inches and greater, environmentally induced flaw growth occurred at flaw depths less than 90 percent of the thickness at σ_{MDOP}.

3. Cyclic flaw growth rates at stress levels and stress ratios applicable to the SM/EPS cryo-hydrogen tank are essentially zero.

FOREWORD

As a result of the Apollo 13 Service Module/Electrical Power System (SM/EPS) LOX tank failure, NASA requested the Aerospace Group of the Boeing Company to perform an experimental study to determine the crack growth behavior of 5Al-2.5Sn(ELI) titanium in a low pressure hydrogen environment as applicable to the Apollo SM/EPS cryo-hydrogen tank. This program was performed under NASA Contract NAS 9-11435 during the period from October 7, 1970 to February 5, 1971 and the results are reported herein. The work was administered under the direction of S. V. Glorioso at NASA/MSC.

Boeing personnel who participated in this investigation include J. N. Masters, Program Leader, and W. D. Bixler/W. L. Engstrom, Technical Leaders. Structural testing of specimens was conducted by A. A. Ottlyk, C. C. Mahnken and G. E. Vermilion. Metallurgical and welding support was provided by H. A. Johnson, T. J. Bosworth and W. C. Butterfield. Don Good prepared the art work.

The information contained in this report is also released as Boeing Document D180-12854-1

TABLE OF CONTENTS

LIST OF ILLUSTRATIONS

LIST OF TABLES

LIST OF TABLES (Cont.)

1.0 INTRODUCTION

The objective of this investigation was to determine the crack growth behavior of 5Al-2.5Sn(ELI) titanium in a low pressure hydrogen environment as applicable to the Apollo Service Module/Electrical Power System (SM/EPS) cryo-hydrogen tank. Precracked surface flaw tests were conducted as indicated below:

TEST		SPECIMENS TESTED [1]				
Temp.	Environment	Tensiles	Static Fracture	Sustained	Load/Unload	Cyclic
70°F	Air	BM WC WH	BM WC WH			
	GH_2 At 300 psia			BM WC WH		BM WC
-200°F	Air/GN_2	BM WC WH	BM WC WH		BM WC	BM WC
	GH_2 At 300 psia			BM WC WH	BM WC	BM WC
-423°F	LH_2	BM WC WH	BM WC WH		BM	BM WC
	GH_2 At 300 psia			BM WC WH		

In addition, welded lack-of-penetration panels were also tested as indicated below:

TEST		SPECIMENS TESTED [1]		
Temp.	Environment	Static Fracture	Sustained	Load/Unload
70°F	Air	WC		WC
	GH_2 At 300 psia		WC	
-200°F	GH_2 At 300 psia		WC	

[1] BM = Base Metal specimens
WC = Weld Metal specimens, flaws in centerline (℄)
WH = Weld Metal specimens, flaws in heat affected zone (HAZ)

2.0 BACKGROUND

The prediction of failure mode, and the estimation of minimum structural life of metallic pressure vessels requires understanding of three major factors. These are the initial flaw sizes, the critical flaw sizes (i.e., the sizes required to cause fracture at a given stress level), and the subcritical flaw growth characteristics.

2.1 Critical Flaw Sizes-Failure Mode

The failure mode of a pressure vessel is dependent upon the fracture toughness of the material, thickness, and the applied stress level. For combinations of these variables in which the critical flaw size is small with respect to thickness, the failure mode is complete fracture, and the vessel is termed "thick walled".

For surface flaws in uniformly stressed "thick walled" vessels, the critical flaw sizes can be calculated using the expression:

$$(a/Q)_{cr} = \frac{1}{1.21\pi}\left(\frac{K_{Ic}}{\sigma}\right)^2 \qquad (1)$$

where:
- a = depth (semi-minor axis) of a semi-elliptical surface flaw
- Q = flaw shape parameter (see Figure 1)
- σ = uniform stress applied perpendicular to the plane of crack
- K_{Ic} = plane strain stress intensity factor or fracture toughness of the material.

Figure 2 is a graphical representation of Equation (1).

If the critical flaw sizes approach or exceed the wall thickness, the vessel is termed "thin walled". In order to predict critical flaw sizes as well as failure modes and operational life of "thin walled" vessels, it is necessary to know the stress intensity for flaws which become very deep with respect to the wall thickness. The stress intensity solution for semi-elliptical surface flaws shown in Equation (1) was derived by Irwin (Reference 1) and has been found to be reasonably accurate for flaw

depths up to about 50 percent of the material thickness. At greater depths, the applied stress intensity is magnified due to the effect of the free surface near the flaw tip. This means that in "thin walled" vessels the flaw tip stress intensity can attain the critical value (i.e., the K_{Ic} value) at a flaw size which is significantly smaller than that which would be predicted using Equation (1).

Kobayashi (Reference 2) has developed an approximate solution for deep surface flaws which are long with respect to their depth (i.e., small a/2c values). The results are shown in terms of a stress intensity magnification factor (M_K), versus a/t in Figure 3. This factor is applied to the original Irwin equation to obtain the stress intensity for deep surface flaws. As Figure 3 illustrates, the magnification reaches a maximum value of about 60 percent. Experimental data obtained on several materials appears to provide a fair degree of substantiation to the available solution (References 3 and 4) for flaws of moderate aspect ratios (i.e., a/2c values from 0.10 to 0.20). Kobayashi's solution tends to slightly underestimate the magnification for longer flaws.

Kobayashi's original solution was limited to depth-to-thickness ratios (a/t) of 0.70. The curve was later extended to greater depths for engineering use (i.e., the dotted part of Figure 3) as substantiating data became available. In Reference 4 it was found that use of this type of a solution was practical up to the point where the plastic zone ahead of the flaw tip[1] becomes very large with respect to the remaining unbroken ligament (t_n). For shallow flaws in brittle materials, the fracturing process is very abrupt. The amount of flaw growth prior to failure, under a rising load, can usually be considered to be negligible. In this case, all important dimensions (i.e., a and ρ) are small with respect to thickness. However, as the plastic zone becomes large (e.g., $\rho/t_n \rightarrow 1.0$), important deviations occur. Foremost of these is that large amounts of stable crack extension can occur, under rising load, well before complete fracture. An example of this behavior is illustrated in Figure 4.

[1] The plastic zone size herein is estimated as $\rho = \frac{\pi}{16}\left(\frac{K_{Ic}}{\sigma_{ys}}\right)^2$

This figure, from Reference 5, shows the amount of flaw extension which takes place in 2219-T87 aluminum weldments. These specimens were loaded to a predetermined stress level and then the load was rapidly dropped to zero. After fatigue marking the flaw front and failing the specimens, the growth-on-loading was measured directly from the fracture face. Significantly, in fatigue tests at constant maximum stress this growth-on-loading appears to occur only on the first cycle. Growth on subsequent cycles proceeds at a much lower rate. Similar observations have been made for 2219-T87 aluminum weldments at -320 and -423°F (Reference 4) and for titanium alloys (References 4 and 6). In the extreme case, this slow flaw growth can result in the flaw growing completely through-the-thickness. The specimen finally fails, upon a further increase in load as a through-the-thickness crack. In this instance, of course, the surface flaw solutions are not meaningful in describing the fracture process. As would be expected, predicted failure stresses based upon plane stress data and the original surface flaw length (not depth) correspond quite well (Reference 4). This is shown in Figure 5. The solid curve represents the conventional stress-flaw size relation for through cracks in a titanium alloy for an experimentally determined K_{CN} value of 104.7 ksi $\sqrt{\text{in.}}$. The curve is based upon a finite width specimen of 4.0 inches, equal to the width of surface specimens tested. Data points for the surface flaw specimens are plotted in terms of gross failure stress versus initial flaw length (2c). The correspondence is seen to be good until, of course, net section stress begins to approach the yield strength.

The above noted examples fall into the category of "thin walled" tankage and are normally considered to be the type in which the predicted failure mode is leakage. There are, however, combinations of flaw lengths and depths with which a ductile fracture before leakage could possibly occur. This would require a very deep flaw (i.e., $\rho/t_n \rightarrow 1.0$) whose length was effectively that of a critical through crack length at the applicable operating or proof stress level.

2.2 Subcritical Flaw Growth

An initial subcritical flaw $(a/Q)_i$, as shown in Figure 2, can grow to critical size $(a/Q)_{cr}$ due to fatigue (cyclic stress) and environmentally induced sustained stress

growth. Also, if the initial flaw is large with respect to the critical size, sustained growth may occur in a relatively inert environment.

The growth of an initial flaw to critical size is normally predicted in terms of cycles or time at load from the results of fracture specimen tests and fracture mechanics analysis. It has been shown (References 7, 8 and 9) that for a given environment and cyclic loading profile that the time or cycles to failure depends primarily upon the magnitude of the initial stress intensity (K_{Ii}) as compared to the critical stress intensity, K_{Ic} (i.e., cycles or time to failure = $f(K_{Ii}/K_{Ic})$).

The most important characteristic observed in all sustained stress flaw growth experiments performed to date is the existence of a threshold stress intensity level for a given material in a given environment. This stress intensity is designated as K_{TH}. The observation has been that, below a given stress intensity, flaw growth has not been detected and above this value, growth does occur and can result in fracture or leakage. Threshold values vary widely and have been found to be affected by alloy, heat treat level, grain direction, material form (e.g., base metal and weldment), temperature, and environment.

Considerable experimental and analytical work has been performed on the problem of fatigue crack growth (References 7, 8, 9, 10, 11, 12, 13 and 14). Much of this work has involved study of the effect of varying stress intensity ratios, R (i.e., $R = K_{min}/K_{max}$). It has been observed that cyclic crack growth rates decrease rapidly as R starts to exceed values of about 0.80 to 0.90. Figure 6 taken from Reference 14 illustrates this point. The experimental points shown are from thin surface flaw tests of 6Al-4V titanium.

2.3 Initial Flaw Sizes - The Proof Test

As noted in Paragraph 2.2, the growth of subcritical flaws has been found to be primarily dependent upon the magnitude of the initial stress intensity as compared to the critical value. A successful proof test to a load level above the operating level provides an indication of the maximum possible initial to critical stress

intensity ratio. This maximum stress intensity ratio is related to the proof test factor, α , as follows (Reference 9).

$$\text{max.} \quad (K_{Ii}/K_{Ic}) = 1/\alpha \tag{2}$$

The effect of material thickness on the information gained in a proof test is illustrated schematically in Figure 7. As noted there are three general cases of interest:

I. The critical flaw depth for relatively long (i.e., Q→1.0) surface flaws at the proof and operating stress levels are less than the wall thickness;

II. The critical flaw depth of a relatively long surface flaw is less than the thickness at the proof stress level, but at operating stress level it exceeds the wall thickness;

III. The critical depth of relatively long surface flaws at the proof and operating stress levels exceed the wall thickness.

In the first case, the predicted fracture mode would be catastrophic at both the proof and operating stress levels if failure should occur. In case II, the predicted failure mode at proof stress level is catastrophic and at operating stress level it is leakage. In either case the allowable K_{Ii}/K_{Ic} ratio is less than the K_{TH}/K_{Ic} ratio to allow for cyclic growth to the extent necessary to prevent service operation at or above the K_{TH}. In the third case either the material has such a high toughness or the vessel wall is so thin that flaws cannot attain critical size at either the proof or operating stress level. Consequently, the predicted failure mode at both the proof and operating pressure is leakage. With regard to the maximum possible initial flaw size that could exist in the vessel after a successful proof test, all that can be said is that it is less than the wall thickness, otherwise the vessel would have leaked during the test. [1]

[1] With regard to the case of a very long and deep flaw which might be approaching criticallity as an effective through crack (see Paragraph 2.1), it does appear that the proof test can provide some assurance that service failure will not occur by this mode, (i.e., K_I/K_C in operation $\approx 1/\alpha$)

Obviously, in this case the proof test does not provide assurance against leakage due to multiple pressure cycles, since the initial flaw that was nearly through-the-thickness could grow through in a very few number of operational cycles. However, if the threshold stress intensity, K_{TH} to critical stress intensity ratio is used as the maximum allowable K_{Ii}/K_{Ic}, the proof test should provide some assurance against leakage during a single prolonged operational cycle.

3.0 MATERIALS

One hemispherical SM/EPS cryo-hydrogen tank forging made of 5Al-2.5Sn(ELI) titanium was supplied by NASA/MSC Houston, Texas, to conduct this investigation. The forging was about 0.30" thick with a diameter of 28" as illustrated in Figure 8. This forging was used to obtain base metal and weld metal heat affected zone (HAZ) specimens.

In addition, two 5Al-2.5Sn(ELI) titanium plates, 0.188" thick x 24" x 72", were supplied by NASA/Lewis from Contract NAS 3-12044. The plate material was used to fabricate lack-of-penetration specimens, weld centerline specimens and the grip ends for base metal and weld metal HAZ specimens.

The high purity hydrogen used in these tests was supplied by Airco in the form of K cylinders at about 2000 psi. An analysis of the gas present in the test system was performed by Airco and found to meet the purity requirements of MSFC-SPEC-356, Table IA as indicated in Table I.

4.0 PROCEDURES

4.1 Specimen Fabrication

Precracked surface flawed specimens were used to determine the basic flaw growth characteristics applicable to the SM/EPS cryo-hydrogen tank. Overall dimensions of the specimens were tailored to the size and shape of the available forging as illustrated in Figure 8. Because of the limited amount of forging material available, specimens were made from 5Al-2.5Sn(ELI) titanium plate material or by welding plate to forging material. All welding was performed in a vacuum using a 60 KV Sciaky Electron Beam (EB) welding machine as shown in Figure 9.

Specifically, base metal (forging) specimens were made by EB butt-welding a piece of titanium plate to each end of a piece of tank forging as shown in Figure 10. Weld metal heat affected zone (HAZ) specimens were made by EB butt-welding a piece of titanium plate to a piece of tank forging as shown in Figure 11. Two specimen halves, thus formed, were further machined to a thickness of 0.088" in the test area to simulate actual tank material thickness prior to welding. These halves were then welded together. The weld schedule used on the specimens varied somewhat from that used on the actual SM/EPS cryo-hydrogen tank, since available Boeing equipment has lower voltage, higher amperage capability than that used on the tank. A typical micrograph of the actual tank weld was obtained from NASA/MSC and weld settings were arrived at that would closely simulate this weld. A photomicrograph of the weld along with weld settings used is shown in Figure 13. Weld metal centerline (℄) specimens were made in a similar manner by machining plate material specimen halves to 0.088" thickness in the test section and EB welding them together as described above, and as shown in Figure 12. Final machining as shown in Figures 10, 11 and 12 was then accomplished. The final machined thickness, in the test sections, of the base metal forging and weldment specimens was 0.044" and 0.061", respectively, which was representative of the actual tank wall thicknesses.

Surface flaws were introduced into the fracture specimens by using an electrical discharge machine (EDM) to form a starter notch. After forming the starter notch,

the specimens were cleaned with naptha. Fatigue extension of the starter notch was accomplished by low stress/high cycle tension-tension fatigue. The final flaw shape was approximately semi-elliptical with a flaw depth to length ratio (a/2c) targeted at 0.10. Fatigue extension was accomplished at a gross stress ranging between 20 and 30 ksi, and a stress ratio, R, of 0.06. A cycling frequency of 1800 cpm was used. From 2000 to 36,000 cycles were required, depending upon the initial notch dimensions, the sharpness of the starter notch and whether or not the material was forging or weldment. All precracking was done in air at room temperature. The flaws put in the welded specimens were located in the ℄ and HAZ. These flaws were introduced from the top side of the weld and the flaws in the HAZ were located 0.029" from the weld ℄.

Lack-of-penetration specimens were made by machining plate material into specimen halves and EB welding these halves together as shown in Figure 14. These specimens were machined to the 0.061" thickness before welding, and they were tested in the as-welded condition. An attempt was made to fabricate flaws by terminating the full penetration pass for a predetermined distance and then covering the entire width of the specimen with a cover pass. The specimens fabricated in this manner showed that the combination of high vacuum and high local heat (during the cover pass) would cause diffusion bonding where a crack was desired. Therefore, the rest of the specimens were welded in the normal manner and an EDM notch was machined after welding. These lack-of-penetration specimens were not precracked prior to testing.

4.2 Test Setups

All non-hazardous tests were conducted in an environmentally controlled laboratory at the Boeing Space Center. Tests conducted at -200°F employed the environmental control system shown schematically in Figure 15. A thermocouple mounted on the specimen in the immediate vicinity of the flaw was used to determine the specimen temperature. By manual control of gaseous and liquid nitrogen supplies, any temperature between -320°F and 70°F can be maintained. All non-hazardous static tests were conducted in a 120,000 lb. Baldwin universal testing machine. Non-hazardous cyclic tests were run in a 60,000 lb. hydraulic test machine fabricated by Boeing.

Hazardous tests involving gaseous or liquid hydrogen at 70°F, -200°F and -423°F were conducted at Boeing's remote Tulalip Test Site. The system utilized is illustrated in Figure 16 and the installed specimen is shown pictorially in Figure 17. The cleanliness and integrity of the system was maintained by the use of alternate vacuum and pressure purging, as well as leak checking the system with a CEC Model 120A helium mass spectrometer. Sensitivity of the leak detector was characteristically 4×10^{-10} atm cc/sec of helium. To prevent the possibility of contamination by the vacuum pump oil back-streaming into the hydrogen system, a liquid nitrogen cooled trap was used. The hydrogen system was alternately evacuated and pressurized 3 times each time a specimen was changed. Evacuation was approximately 1×10^{-3} Torr measured at the vacuum pump while pressurization was to 300 psia. A gas sample was removed from the system at a location which required the gas to pass through the specimen cup before entering the sample bottle.

Hydrogen gas regulated down to 300 psia was supplied to a small cup mounted on the specimen. A cup with a pressure transducer pickup was also mounted on the backside of the specimen to sense the pressure rise occurring if the flaw grew through-the-thickness. The cups used are shown installed on a weld metal surface flawed specimen in Figure 18. Hydrogen gas was also supplied to the flaw area of the lack-of-penetration specimens by pressure cups. These cups were necessarily larger because of the increased flaw size of the lack-of-penetration specimen compared with the surface flawed specimen flaw sizes. The pressure on the flaw side was maintained at 300 psia while the backside pressure was held at 290 psia. This was done in order to reduce the local specimen bending caused by the pressure and it still permitted detection of flaw growth through-the-thickness.

The cryogenic temperature conditioning system used on -200°F tests was similar to that used with the non-hazardous testing. As schematically shown in Figure 19, gaseous and liquid nitrogen were mixed at a three-way valve, thereby providing the desired temperature at the cryostat. For tests conducted at 70°F, thermocouple controlled Coates heaters were used. Hazardous surface flawed specimen sustained tests at 70°F and -200°F were conducted in 30,000 lb. dead load fixtures fabricated by

Boeing. Cyclic tests were run in an 80,000 lb. Research Inc. testing machine. All -423°F tests and the lack-of-penetration sustained tests were conducted in a 400,000. lb. Richle Universal testing machine. The pressure and temperature conditioning apparatus for these tests was similar to that described above; however, the -423°F tests utilized liquid hydrogen as a coolant. In all tests, the test temperature was maintained within ± 10°F and the pressure within ± 10 psi. Static tensile specimens tested at -423°F were loaded at a rate to produce failure in about 2 minutes.

4.3 Experimental Approach for the Fracture Tests

All surface flawed specimens were tested with a targeted flaw shape $(a/2c)_i$ of 0.10. Static fracture specimens were tested in air at 70°F, air/nitrogen at -200°F, and liquid hydrogen at -423°F. They were loaded to failure in about one to two minutes. The static specimens were instrumented with pressure cups described above to determine if and when flaw growth through-the-thickness occurred prior to failure. A pressure differential of 15 psi was used during static tests.

In order to determine what combinations of flaw size and stress level caused flaw growth, specimens of various flaw depths and stress levels were sustain loaded at the three test temperatures of interest. The proof and operating stresses were based on a spherically shaped vessel having a 28.3" diameter. Sustained load times varied from 3.5 hours to 113.5 hours with the majority of specimens loaded for approximately 20 hours. Flaw growth through-the-thickness was detected by the use of the pressure cups described above. If failure did not occur, the specimen was unloaded and low stress cycled in air to mark the flaw front and then pulled to failure. Evidence of growth was then observed by a separation between the initial fatigue crack extension and that of final marking. In conjunction with this procedure, it became necessary to separate the environmentally induced flaw growth from growth-on-loading as discussed in Paragraph 2.1. This was accomplished by loading surface flawed specimens to predetermined stress levels and then immediately dropping the load to zero and observing the fracture face for growth after marking and failing the specimen. Specimens specifically utilized in determining growth-on-loading are termed load/unload specimens.

Cyclic specimens were instrumented with a clip gage to measure crack opening displacements as shown in Figure 20. The clip gage was spring loaded against knife edges spot welded to the specimen. An expression for the opening displacements of a completely embedded flaw was provided by Green and Sneddon (Ref. 15). The flaw embedded in an elastic solid was subjected to a uniform load normal to the crack surface at infinity. The maximum opening displacement occurs at the diametrical center of the crack and is expressed by the equation.

$$\delta = \frac{4(1-\mu^2)}{E} \cdot \frac{\sigma a}{\Phi} \qquad (2)$$

Although a rigorous solution is not available for flaw opening displacements for a semi-elliptical surface flaw, such displacements should also be proportional to σ and a/Φ for elastic materials. By following Irwin's procedure (Reference 1) to account for the effect of plastic yielding, the flaw opening displacement, δ, for a surface flaw can be approximated by

$$\delta = C \frac{\sigma a}{\sqrt{Q}} \qquad (3)$$

Where C is a constant. The value of C can be determined by knowledge of initial and final flaw sizes and the change in flaw opening displacement as indicated below:

$$C = \frac{\delta_f - \delta_i}{\sigma \left[(a/Q)_f - (a/Q)_i\right]} \qquad (4)$$

Knowing the above constant, the instantaneous flaw size can be estimated and, therefore, the flaw growth rates can be calculated.

Lack-of-penetration tests were conducted at various $(a/2c)_i$ ratios to simulate very long flaws. Static tests were run in air at 70°F to determine if and when the flaw

grew through-the-thickness. Sustained load tests were conducted in 300 psia gaseous hydrogen at 70°F and -200°F. Test durations varied from 4.5 hrs. to 20.0 hrs. After sustained loading, the specimens were failed.

4.4 Stress Intensity Solution

Where stress intensity values are reported, they were based on the following expression:

$$K_I = 1.95\ \sigma\ (a/Q)^{1/2}$$

where

K_I = plane strain stress intensity

σ = gross stress

a = flaw depth

Q = shape parameter

Values of Q are shown in Figure 1.

5.0 TEST RESULTS AND ANALYSIS

5.1 Mechanical Properties

Mechanical property tests were conducted for the 5Al-2.5Sn(ELI) titanium forging and weldments used in evaluating the fracture characteristics of the SM/EPS cryo-hydrogen tank material. These tests were run at temperatures of 70°F in air, -200°F in air/gaseous nitrogen and at -423°F in liquid hydrogen. In addition to the extensometer used to measure strain on the forging and weldment tensile specimens, a strain gage was positioned on the weld nugget of the weldments. The results of these tensile tests are shown in Figure 21. The strength of the 5Al-2.5 Sn(ELI) titanium increases as the temperature decreases for both the forging and weldments. The strength of the weldment was generally higher than the forging, especially at cryogenic temperatures. The detailed results are presented in Table II for the materials.

5.2 Precracked Surface Flawed Specimen Tests

Static fracture tests, sustained load tests and cyclic load tests were conducted using precracked surface flawed specimens fabricated per paragraph 4.1.

5.2.1 Fracture Tests

Static fracture tests of 5Al-2.5Sn(ELI) titanium forging and weldment material were conducted in air at 70°F, in air/gaseous nitrogen at -200°F and in liquid hydrogen at -423°F. The weldment specimens either had flaws located in the ℄ or in HAZ. The results of these tests are presented in Figures 22 through 27, while the detailed data are presented in Tables III, IV and V. In general, the deep flaws (above 85 percent of the thickness) grew through-the-thickness prior to failure as through-the-thickness cracks. This was true for either the forging or weldment, regardless of the test temperature. Except for the -423°F tests, the only specimens which failed prior to growth through-the-thickness did so above the yield strength. No plane strain fractures were obtained at 70°F or -200°F. At -423°F, one forging (BM-6) and one weldment (WH-5) specimen failed below the yield strength (see

Figures 26 and 27) and prior to having the flaws grow through-the-thickness. Excessive flaw growth probably occurred on these specimens based on the amount of growth observed on specimens having similar initial flaw depths and were either loaded/unloaded to lower stress levels or grew through-the-thickness upon loading. Specimens BM-15 and WC-6 support this conclusion, for the forging and weldment respectively. An apparent plane strain fracture toughness, K_{Ic}*, of 53.9 ksi $\sqrt{in}$ (based on the initial flaw dimensions) was obtained for the forging material. This value agrees favorably with other plane strain fracture data generated from thicker test specimens (Reference 8).

The fracture tests do show that the failure mode of either the forging or weldment (in representative tank wall thicknesses) is leakage at 70°F and -200°F at stresses less than the yield strength and that any proof test conducted does not guarantee any maximum possible initial flaw size less than the wall thickness. This is a classic example of a Case III pressure vessel as discussed in Paragraph 2.3. At -423°F, plane strain fracture can occur at stresses below the yield strength but excessive flaw growth will take place. For deeper flaws, plane strain fracture will not occur; the flaws will growth through-the-thickness (leakage failure mode).

These test results also show that the probability of leakage during proof test is remote, because the flaw would have to be deeper than approximately 96 percent of the thickness for either the forging or weldment, regardless of proof temperature (70°F through -423°F).

5.2.2 Sustained Load and Growth-On-Loading Tests

Sustained load tests of 5Al-2.5Sn(ELI) titanium forgings and weldments at temperatures of 70°F, -200°F and -423°F were conducted and the results are presented in Figures 22 through 27. The test environment for all of these tests was high purity gaseous hydrogen at 300 psia. These tests were generally of 20.0 hours duration. The detailed data are presented in Tables VI through XI. Flaw growth was observed in both the forging and weldment materials for particular combinations of stress and flaw depth, but because of the growth through-the-thickness observed with the static fracture specimens additional tests were conducted to separate time dependent, sustained

load flaw growth from growth-on-loading. Key specimens that showed flaw growth after being sustain loaded for 20 hours were duplicated with specimens of similar depth flaws and loaded to the same stress level and then immediately unloaded. These load/unload specimen tests were conducted at the appropriate temperature and the detailed data for these specimens are presented in Table XII. The specimen tests at -200°F did not indicate as much growth as the specimens they duplicated, thereby indicating that part of what was observed as growth in the sustained specimens was environmentally induced growth. This was not the case at -423°F, where the single load/unload specimen demonstrated more growth than the sustain loaded specimen it was intended to duplicate. From this single observation (see Figure 26) it appears that environmentally induced flaw growth did not occur during the -423°F load tests. Time dependent flaw growth was observed at 70°F, with one specimen growing through-the-thickness in 3.5 hours, as illustrated in Figure 22.

Fractographs illustrating the flaw growth observed on sustained loaded and load/unloaded specimens are presented in Figures 28, 29 and 30.

For both the forging and weldment materials at the test temperatures evaluated, it was possible to generate a curve (dashed line on Figures 22 through 27) below which no flaw growth could be expected; either environmentally induced or growth-on-loading. As illustrated in Figures 22 and 23, a flaw would have to be about 83 percent through-the-thickness before flaw growth would occur during a 70°F proof test. This is true for both the forging and weldment material. If proof tests were conducted at colder temperatures, the flaw which would grow during proof would have to be even deeper. No flaw growth would be expected when loaded to the maximum design operating stress (σ_{MDOP}) for flaw depths up to approximately 90 percent of the thickness at the test temperatures evaluated. These observations are based on flaws that had an a/2c=0.10.

It should be pointed out that after these no flaw growth curves were defined by 20 hour sustained tests, specimens with about 83 percent deep flaws were loaded to proof stresses and held for about 5 days. No flaw growth was observed on these specimens. These tests were run with both forging and weldment materials at temperatures of 70°F and -200°F.

In summary, environmentally induced flaw growth was observed at 70°F and -200°F for the 5Al-2.5Sn(ELI) titanium and gaseous hydrogen material/environment combination, while none was observed at -423°F. The environmentally induced flaw growth that was observed, occurred at stresses exceeding the proof stress.

5.2.3 Cyclic Tests

Cyclic flaw growth tests were conducted at 70°F, -200°F and -423°F for both the forging and weldment materials. These specimens were instrumented to determine the flaw opening displacement as described in Paragraph 4.3. These specimens were tested in gaseous hydrogen (70°F and -200°F), air/gaseous nitrogen (-200°F), and in liquid hydrogen (-423°F). Instantaneous cyclic flaw growth rates were calculated from the flaw opening measurements and the results are presented in Figure 31. The cyclic flaw growth rates obtained from the forgings agreed favorably with the weldment data when adjusted to an equivalent stress level. All of the data presented in Figure 31 is for specimens that had initial flaw depths that were 50 percent of the thickness and were cycled to leakage. The detailed data for the cyclic specimens are presented in Tables XIII and XIV.

This cyclic data was then used to generate cycle to leak curves for the forging and weldment materials at temperatures of 70°F, -200°F and -423°F. These curves are presented in Figure 32 for σ_{MDOP} and a stress ratio R, of 0.1. As these curves indicate, it would take a minimum of 3500 cycles to cause leakage with a flaw depth that was initially 90 percent of the thickness. This is a very conservative number, because the actual cyro-hydrogen tank is stressed to a lower stress than σ_{MDOP} during flight and at an R value of 0.86. As Tables XIII and XIV indicate, specimens tested at an R value of 0.86 had as many as 83,400 cycles without detectable flaw growth.

The cyclic flaw growth rates obtained do not appear to be affected by the environment (air versus gaseous hydrogen) because of the flaw sizes and stress levels tested.

at 70°F did not indicate any flaw growth as shown in Figure 34. The detailed data for this load/unload specimen is presented in Table XVIII. A single specimen with a flaw depth that would just get through a proof test (45 ksi) at 70°F without leaking was proof stressed and then sustain loaded in gaseous hydrogen at -200°F. Significant growth was observed on this specimen. Photographs showing typical flaws in these lack-of-penetration specimens are shown in Figure 35.

In summary, it appears that 3.0" long flaws that are less than 57 percent of the thickness would have environmentally induced growth at both 70°F and -200°F when stressed to σ_{MDOP}. Flaws greater than 57 percent of the thickness would be screened by the proof test. With flaws that were only 1.5" long, flaw depths less than 82 percent of the thickness would grow at 70°F and not at -200°F when stressed to σ_{MDOP}. Flaws greater than 82 percent of the thickness would be screened by the proof test.

5.3 Lack-Of-Penetration Specimen Tests

Static fracture tests of 5Al-2.5Sn(ELI) titanium weldments that had simulated lack-of-penetration weld defects were conducted at 70°F. These specimens had surface flaws with lengths of about 1.5" and 3.0" and of various flaw depths. The results of these tests are shown in Figures 33 and 34 while the detailed data are presented in Tables XV and XVI. The flaws were observed to break through-the-thickness prior to failure as a through crack in plane stress. The backside of the specimen (opposite the flaw) was observed visually during loading and very high strains took place in the remaining ligament. An apparent plane stress fracture toughness, K_c^*, of between 150 and 170 ksi $\sqrt{in}$ was obtained. As one might anticipate, the longer the flaw, the lower the gross stress at which flaw break through occurred at a given initial flaw depth. As indicated by Figures 33 and 34, initial flaw depths greater than 82 and 57 percent of the thickness for 1.5" and 3.0" length flaws, respectively, would cause leakage during a 70°F proof. This compares with 96 percent for the precracked surface flaws $(a/2c)_i = 0.10$ discussed in Paragraph 5.2.1.

Sustained load tests were also conducted for specimens having flaw lengths of 1.5" and 3.0". These tests were run at a stress level of 33 ksi (σ_{MDOP}) and at 70°F and -200°F. The sustained load test results for specimens having a flaw length of 1.5" are presented in Figure 33 and Tables XVII and XIX. As Figure 33 indicates, flaws less than 82 percent of the thickness would not leak during proof test (70°F) but would probably grow when exposed to a gaseous hydrogen environment at 70°F and σ_{MDOP}. This is not the case when exposed to gaseous hydrogen at -200°F; the flaw depth would have to be greater than 82 percent of the thickness for environmental growth to take place and that size initial flaw would have caused leakage during proof.

With flaws that were 3.0" in length and less than 57 percent of the thickness, the 70°F proof test would not cause leakage (see Figure 34). Sustain loaded specimens at σ_{MDOP} and with flaws about 57 percent of the thickness would have environmentally induced flaw growth at both 70°F and -200°F. A load/unload specimen

6.0 OBSERVATIONS AND CONCLUSIONS

Some of the major observations and conclusions made from this study are presented below:

1. The failure mode of the SM/EPS cryo-hydrogen tank is leakage at both proof and operating stress levels for temperatures ranging from 70°F to -423°F. This is also true for long, deep flaws (2c = 1.5"→3.0") where the failure mode is leakage rather than a ductile fracture as an effective through-the-thickness crack.

2. Environmentally induced flaw growth was observed in testing 5Al-2.5Sn (ELI) titanium in a low pressure, high purity gaseous hydrogen environment at temperatures of 70°F and -200°F. The time dependent flaw growth that was observed, occurred at stresses exceeding the proof stress. No flaw growth would be expected when loaded to σ_{MDOP} for flaw depths up to approximately 90 percent of the thickness. These observations were based on flaws that were less than about 0.5" long. For flaws that are 1.5" long, environmentally induced flaw growth will not occur at depths less than about 82 percent of the thickness at -200°F when stressed to σ_{MDOP}. For flaws that are 3.0" long, sustained load growth at σ_{MDOP} could occur at depths less than 50 percent of the thickness at temperatures of 70°F and -200°F. No environmentally induced flaw growth was observed at -423°F in hydrogen.

3. Cyclic flaw growth rates at stress levels and stress ratios applicable to the SM/EPS cryo-hydrogen tank (R = 0.86) are essentially zero.

REFERENCES

1. Irwin, G.R.; "Crack Extension Force for a Part-Through-Crack in a Plate", Journal of Applied Mechanics, Vol. 29, Trans. ASME, Vol. 84, Series E, December 1962.

2. Kobayashi, A.S.; "On the Magnification Factors of Deep Surface Flaws", Structural Development Research Memorandum No. 16, The Boeing Company, December 1965.

3. Tiffany, C.F., Masters, J.N., and Pall F.A.; "Some Fracture Considerations in the Design and Analysis of Spacecraft Pressure Vessels", presented at the ASM National Metals Congress, Chicago, October 1966.

4. Masters, J.N., Haese, W.P., and Finger, R.W.; "Investigation of Deep Flaws in Thin Walled Tanks", NASA CR-72606, December 1969.

5. Masters, J.N., Hall, L.R., Finger, R.W.; "Stress Corrosion of Metal Tank Materials", Rough Draft - Interim Final Report, NASA Contract NAS 3-12003, January 1970.

6. Bixler, W.D.; "Comparison of Flaw Growth Characteristics Under Cryogenic Proof and Ambient Test Conditions for Apollo Titanium Pressure Vessels", D2-121700-1, The Boeing Company, January 1970.

7. Tiffany, C.F., and Lorenz, P.M.; "An Investigation of Low Cycle Fatigue Failures Using Applied Fracture Mechanics", ML-TDR-64-53, May 1964.

8. Tiffany, C.F., Lorenz, P.M., and Hall, L.R.; "Investigation of Plane Strain Flaw Growth in Thick-Walled Tanks", NASA CR-54837, February 1966.

9. ASTM Special Committee on Fracture Testing of High-Strength Metallic Materials, "Progress in the Measurement of Fracture Toughness and the Application of Fracture Mechanics to Engineering Problems", Materials Research and Standards, Vol. 4, No. 3, March 1964.

10. Hall, L.R.; "Plane-Strain Cyclic Flaw Growth in 2014-T62 Aluminum and 6Al-4V(ELI) Titanium", NASA CR-72396, November 1968.

11. Roberts, R. and Erdogan, R.; "The Effect of Mean Stress on Fatigue Crack Propagation in Plates Under Extension and Bending", ASME Paper No. 67, WA/MET-2, 1967.

12. Krafft, J.M.; "A Comparison of Cyclic Fatigue Crack Propagation With Single Cycle Crack Toughness and Plastic Flaw", Report to ASTM Fracture Toughness of High Strength Materials Special Committee, September 1965.

13. Forman, R.G., Kearney, V.E., and Engle, R.M.; "Numerical Analysis of Crack Propagation in Cyclic Loaded Structures", Journal of Basic Engineering, Trans. ASME, Series D, Vol. 89, pp. 459-464, September 1967.

14. Masters, J.N.; "Cyclic & Sustained Load Flaw Growth Characteristics of 6Al-4V Titanium", NASA CR-92231, July 1968.

15. Green, A.E., and Sneddon, I.N.; "The Distribution of Stress in the Neighborhood of a Flat Elliptical Crack in an Elastic Solid", Proc. Cambridge Phil. Soc. Vol. 46 (1950).

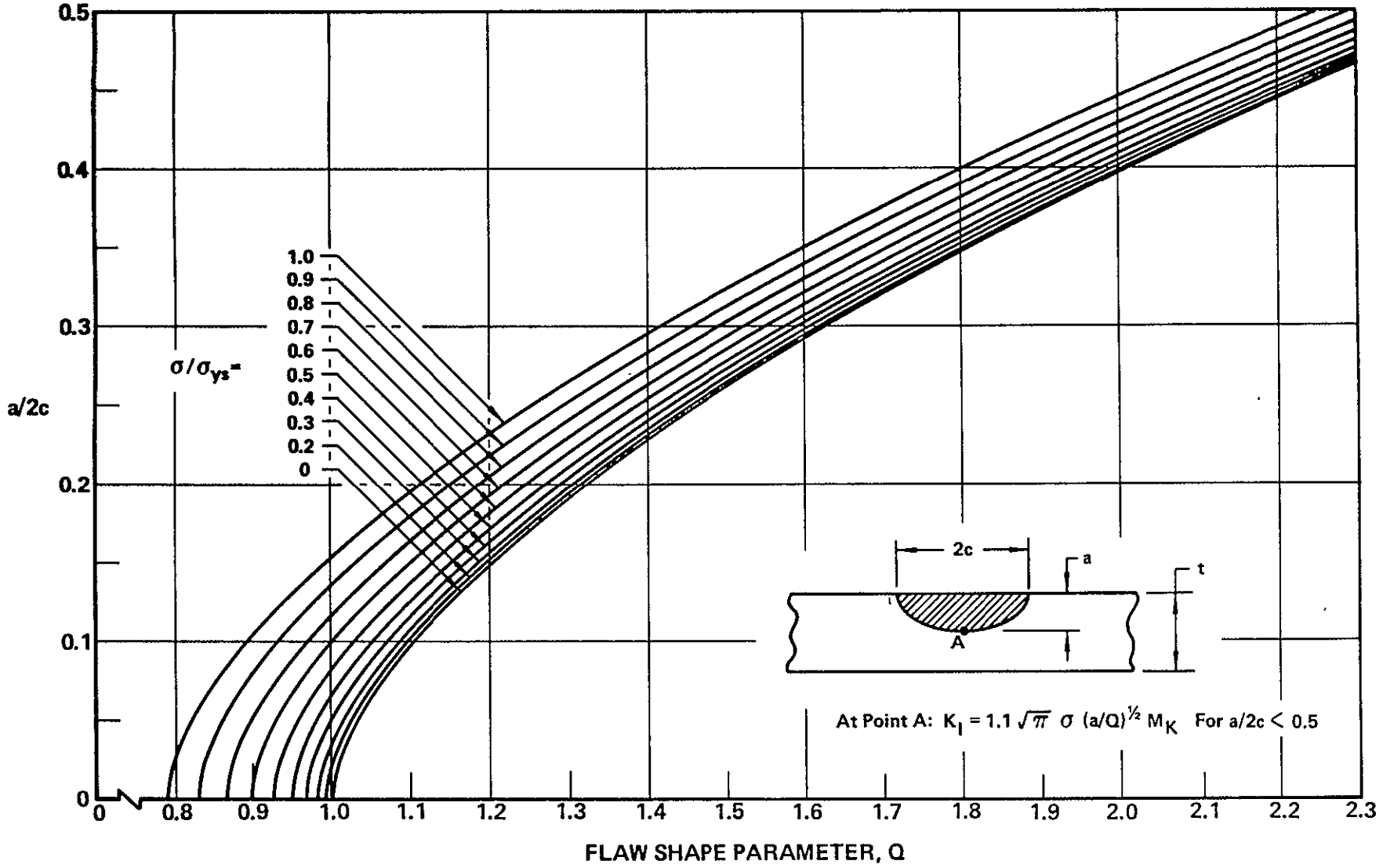

Figure 1: SHAPE PARAMETER CURVES FOR SURFACE AND INTERNAL FLAWS

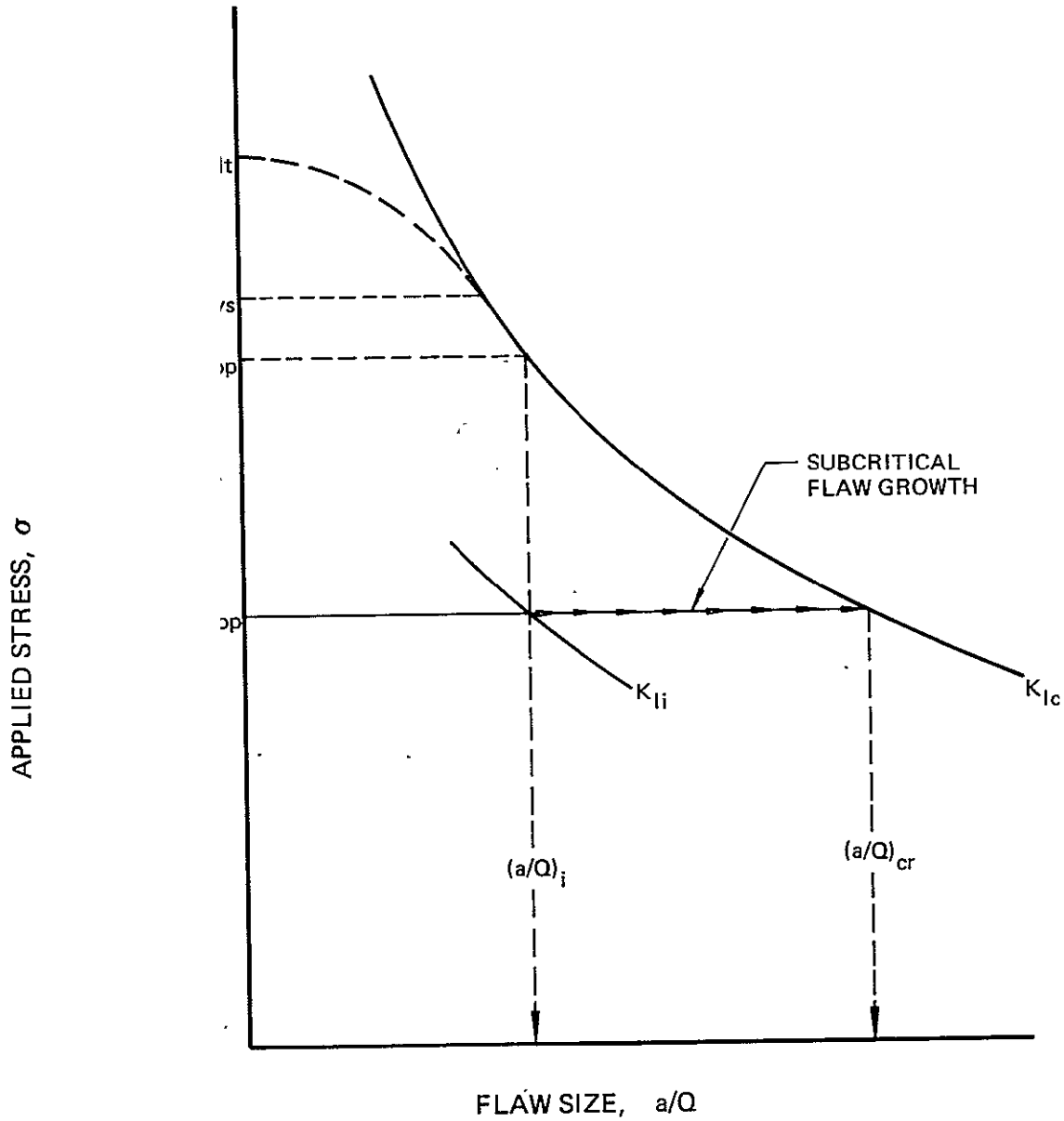

Figure 2: APPLIED STRESS VS. FLAW SIZE

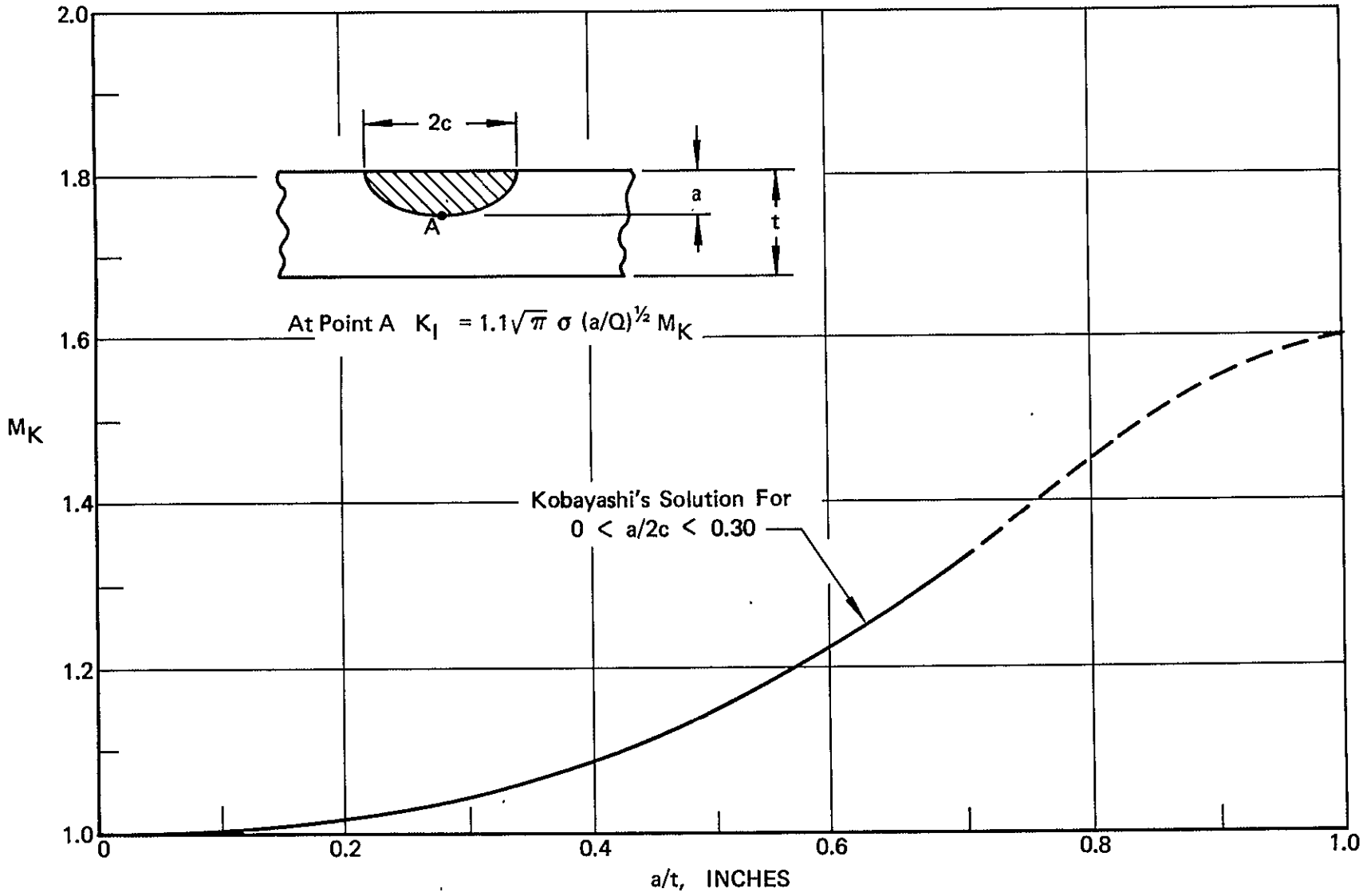

Figure 3: STRESS INTENSITY MAGNIFICATION FACTORS FOR DEEP SURFACE FLAWS

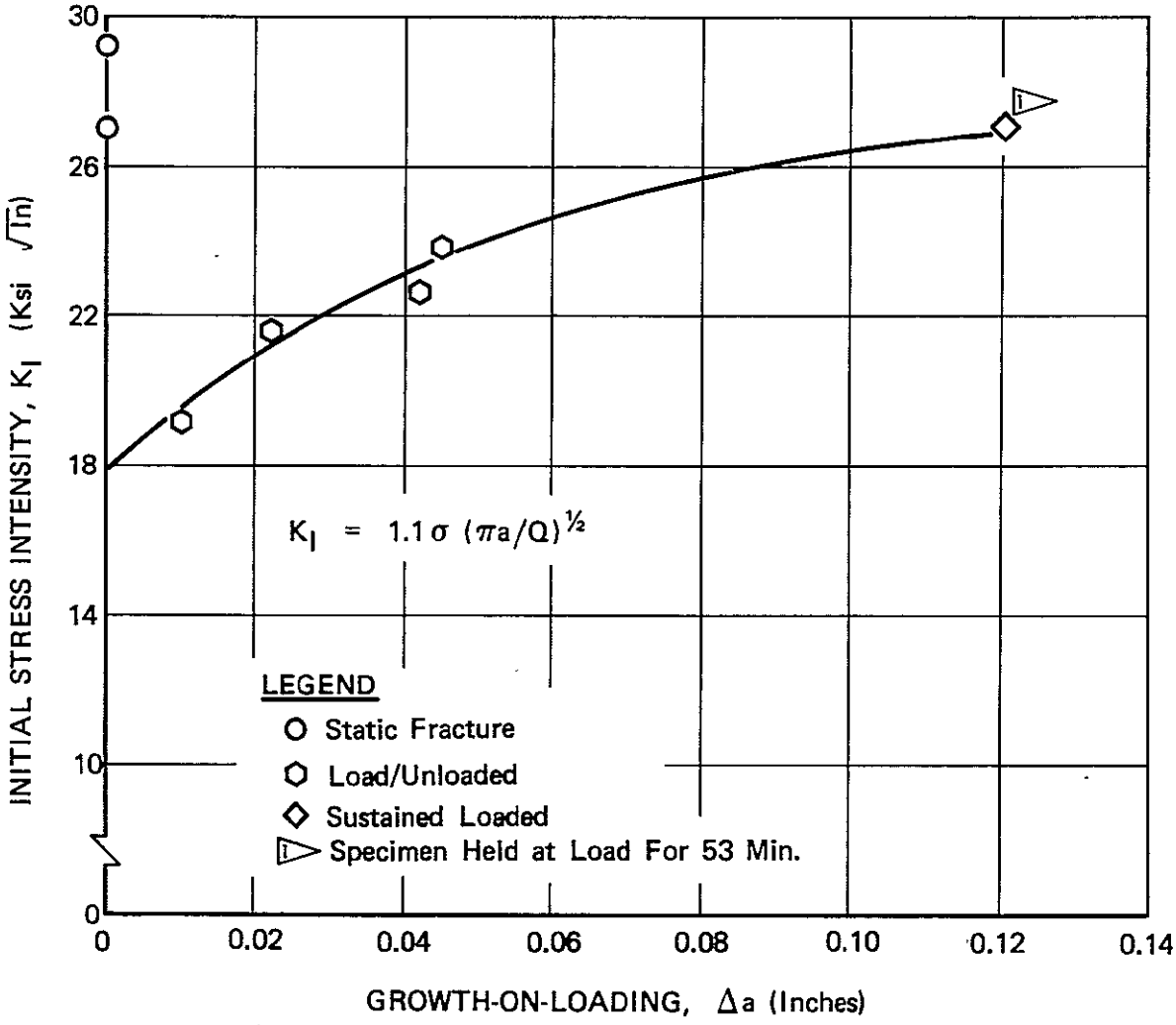

Figure 4: GROWTH-ON-LOADING IN 2219-T87 ALUMINUM WELDMENT IN AIR AT ROOM TEMPERATURE

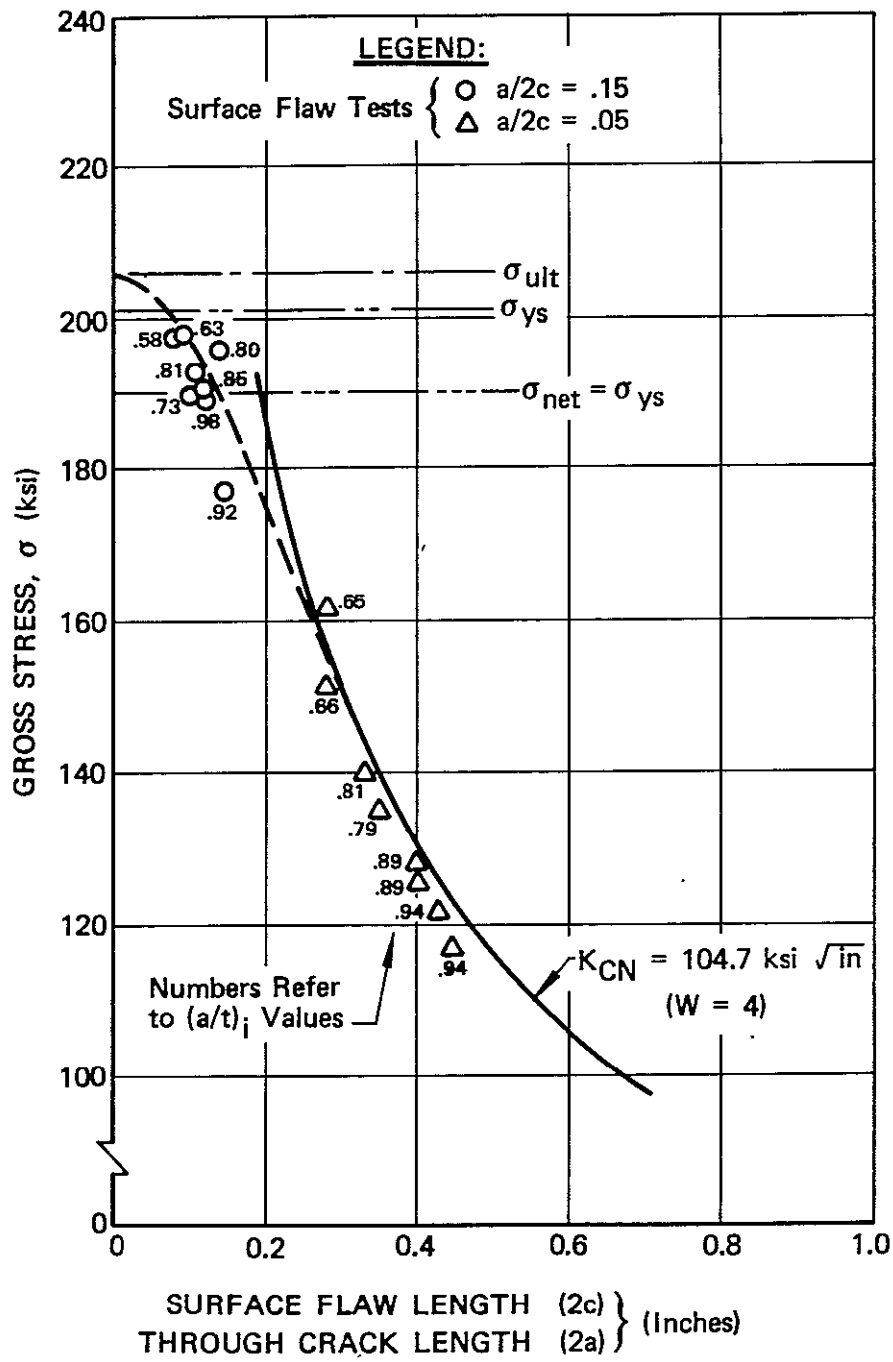

Figure 5: COMPARISON OF SURFACE FLAW & CENTER CRACK DATA (t = 0.020", 5Al-2.5Sn Titanium Base Metal @ -423 °F)

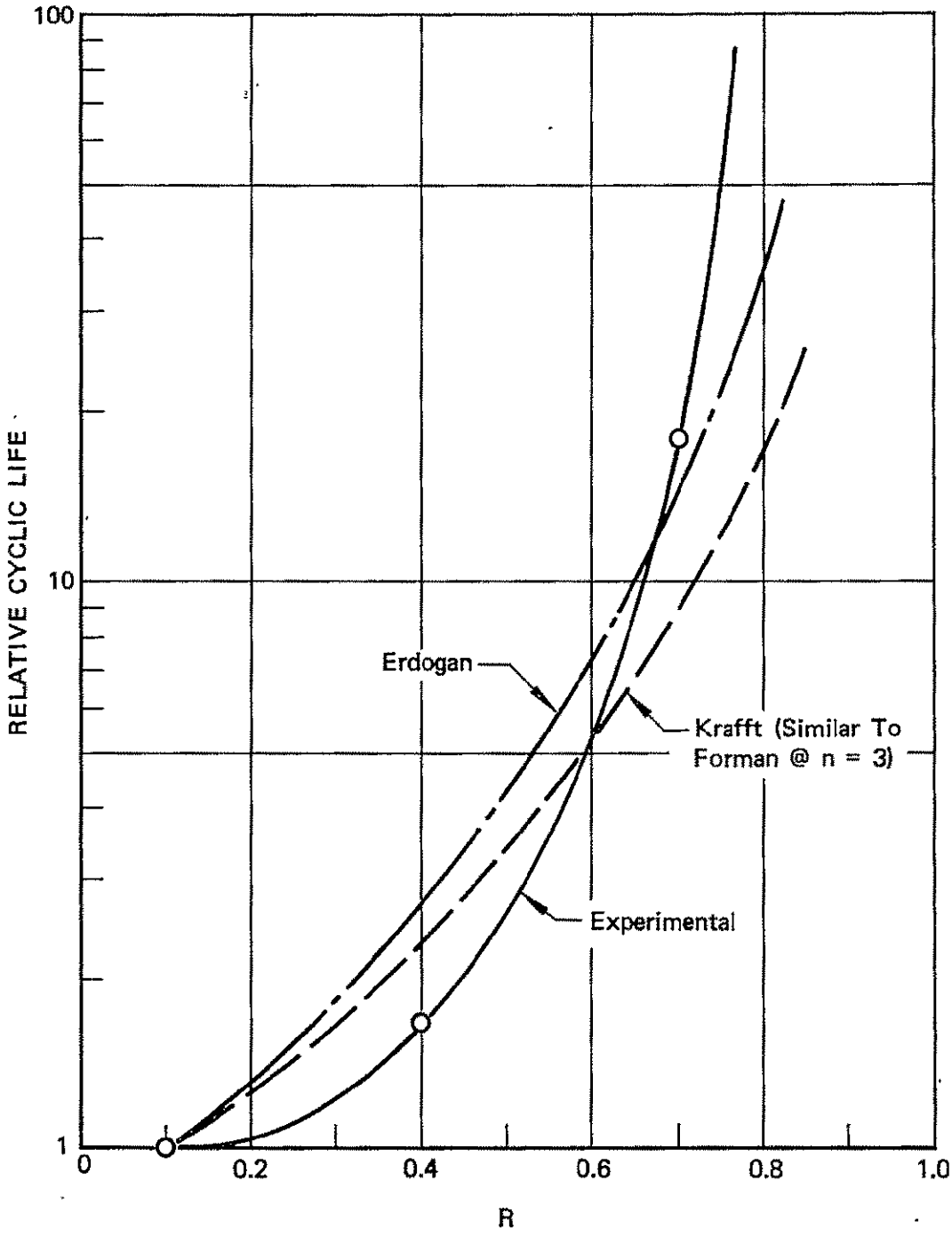

Figure 6: EFFECT OF R VALUE ON CYCLIC LIFE

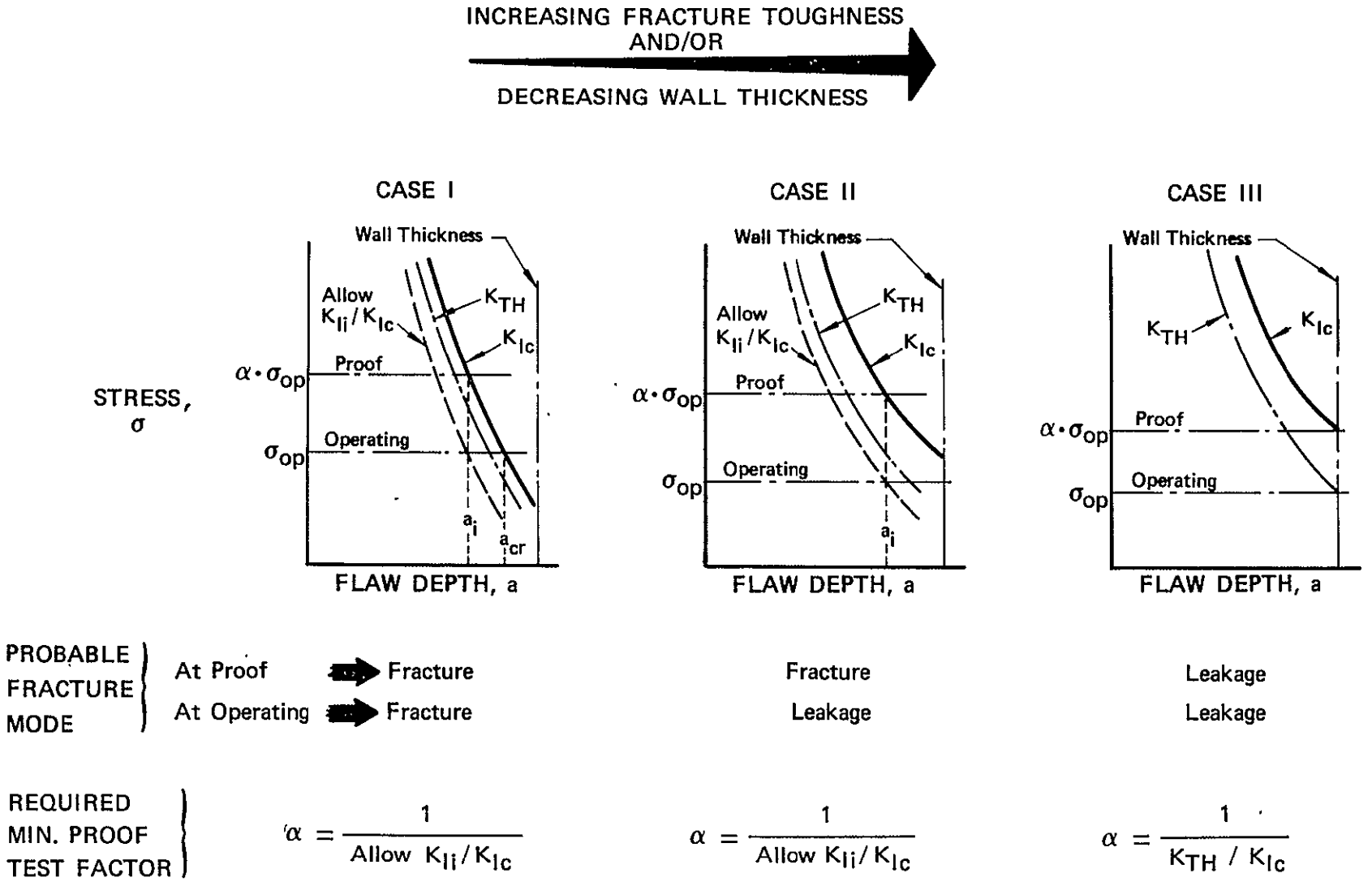

Figure 7: THE EFFECT OF WALL THICKNESS ON THE VALUE OF THE PROOF TEST

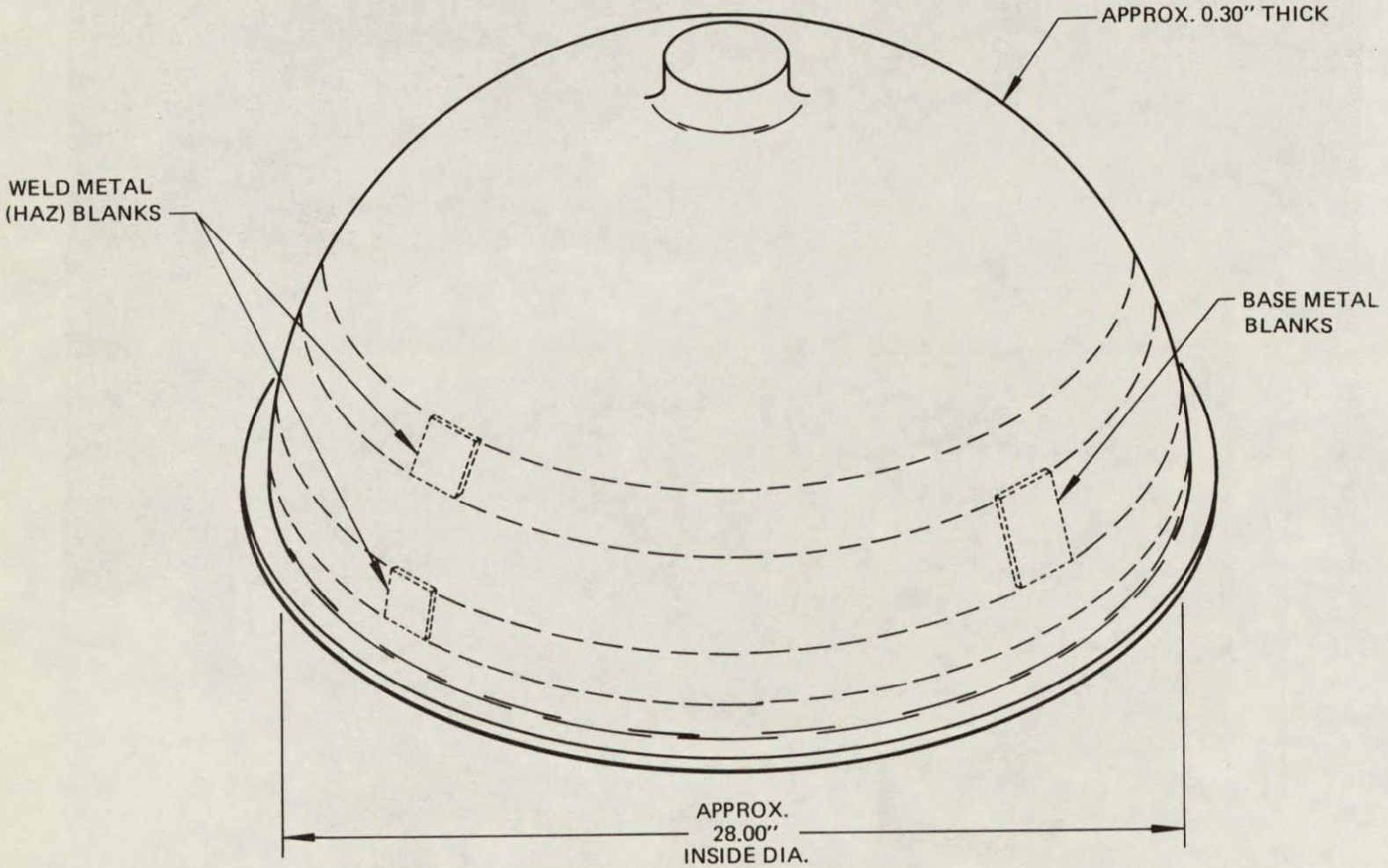

Figure 8 : HEMISPHERICAL SM/EPS CRYO-HYDROGEN TANK FORGING

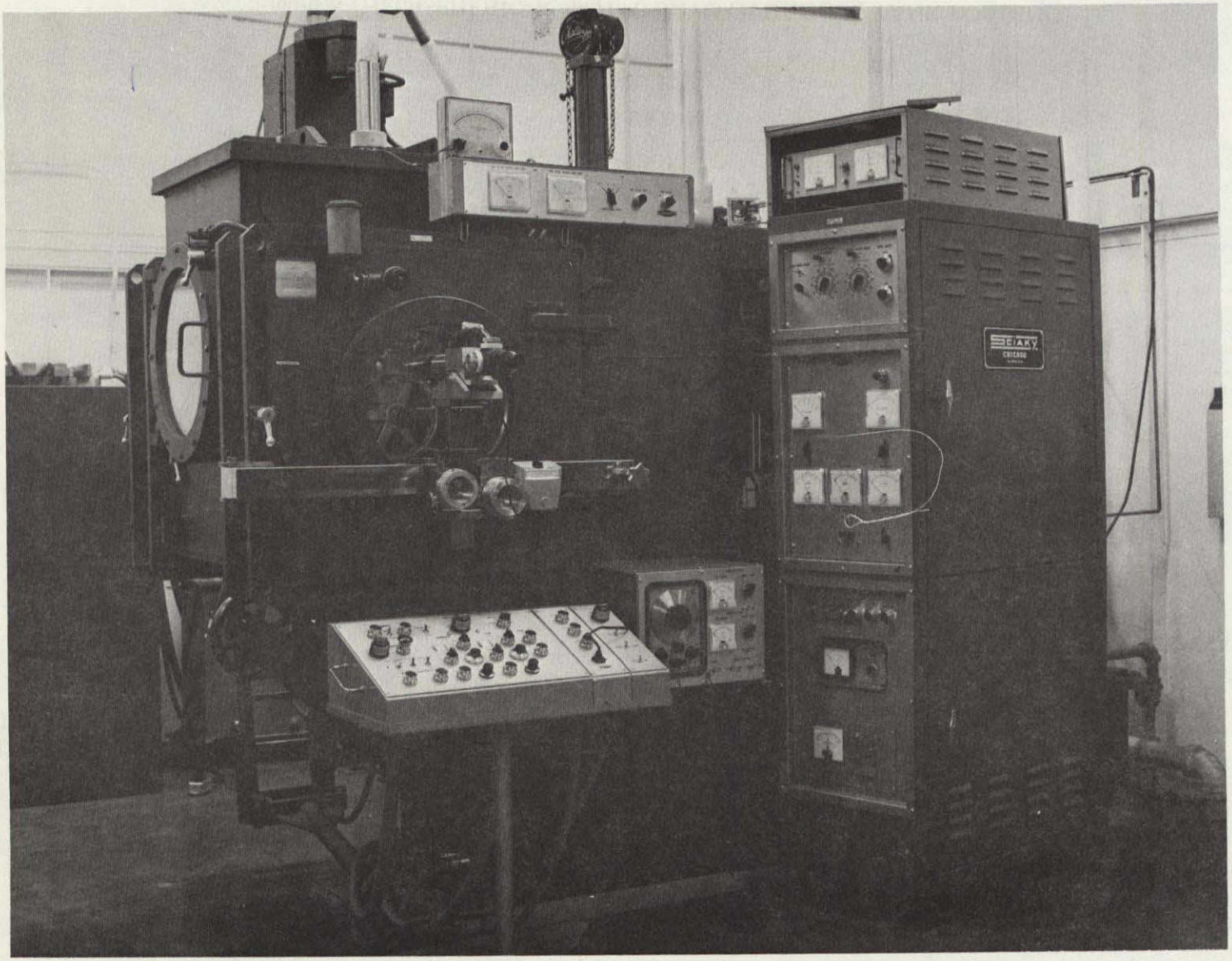

Figure 9 : 60 KV SCIAKY ELECTRON BEAM WELDING FACILITY

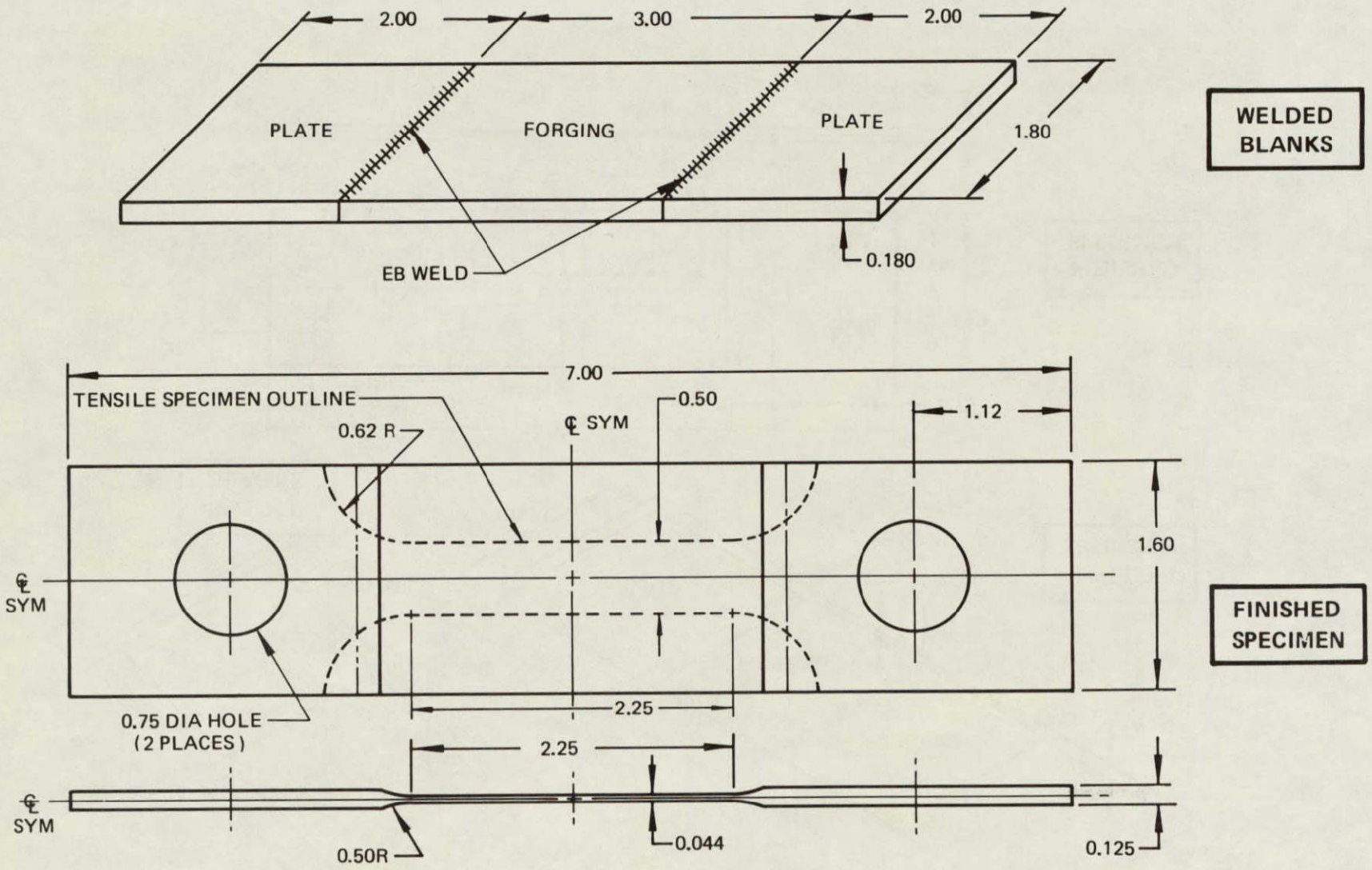

Figure 10 : BASE METAL SURFACE FLAW AND TENSILE SPECIMEN

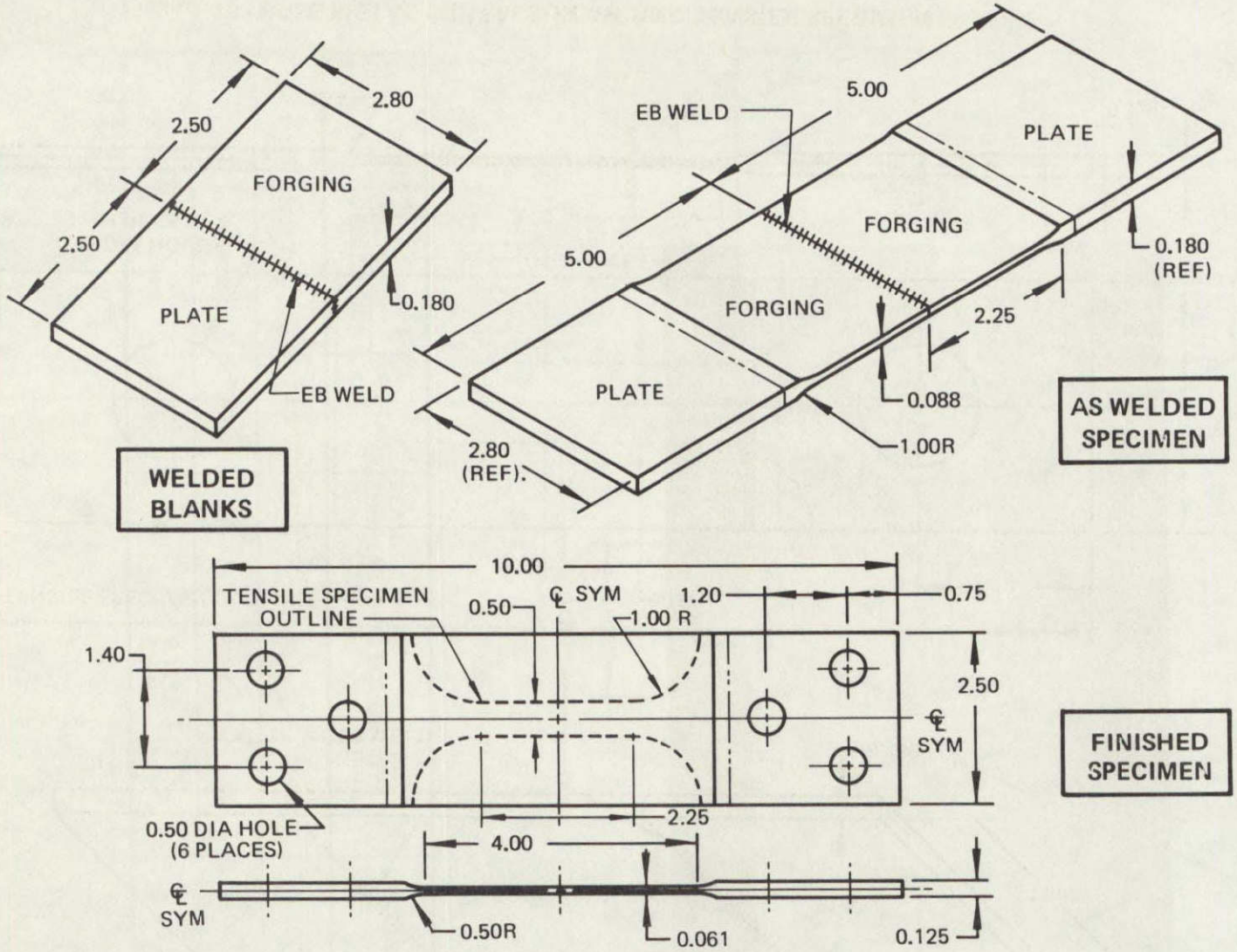

Figure 11: WELD METAL (HAZ) SURFACE FLAW AND TENSILE SPECIMEN

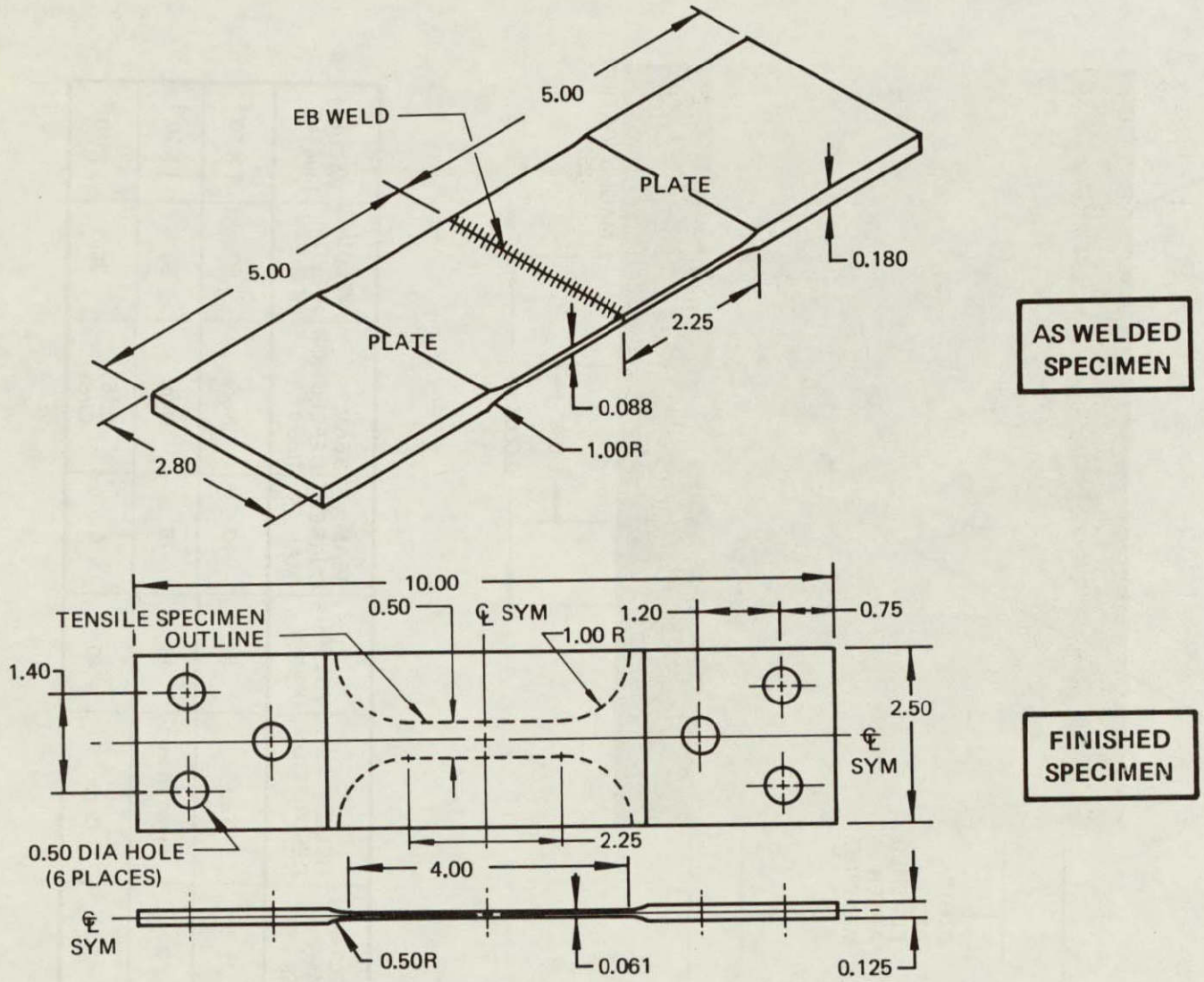

Figure 12 : WELD METAL (℄) SURFACE FLAW AND TENSILE SPECIMEN

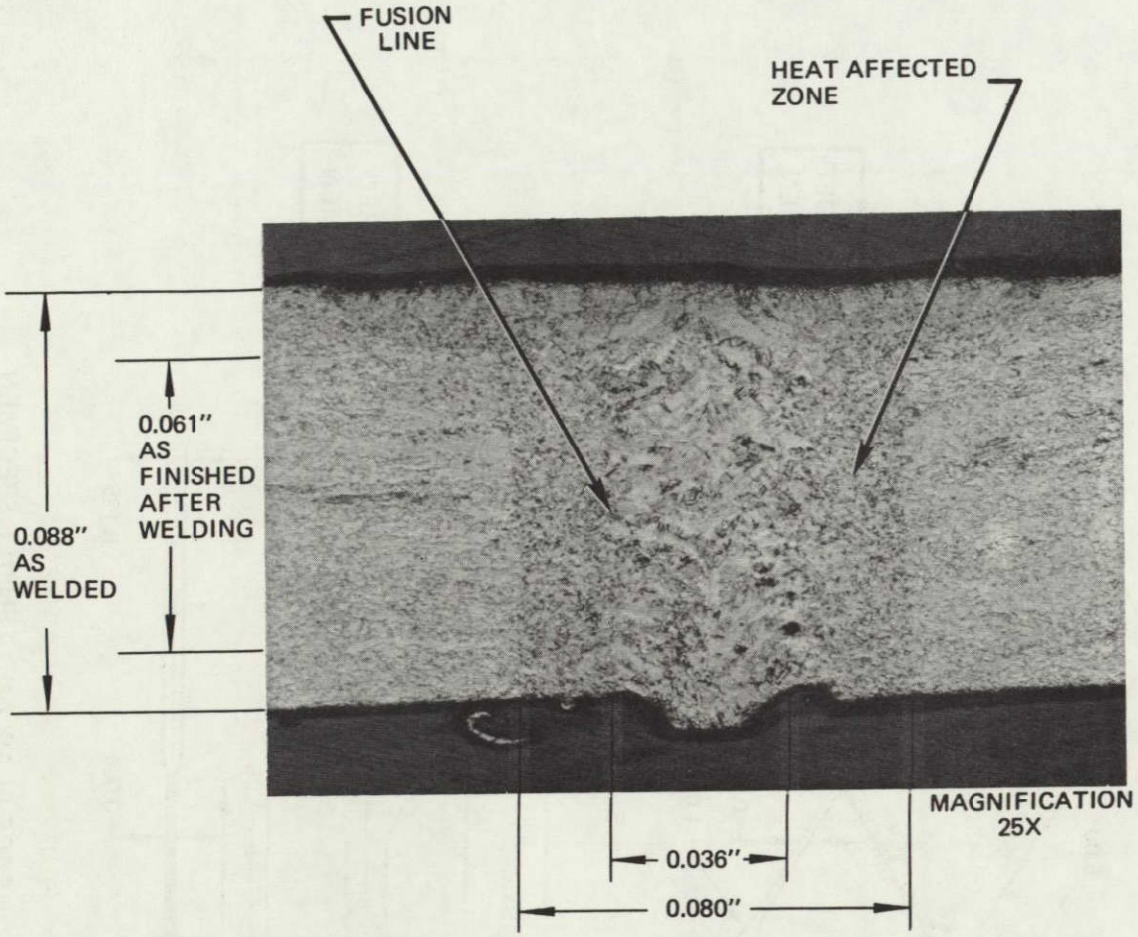

ELECTRON BEAM PASS	WELD DESCRIPTION	VOLTAGE (KV)	BEAM CURRENT (MA)	BEAM DEFLECTION (Inch)	WELDING SPEED (IPM)	VACUUM (mm-Hg)
1	Tack	40	10	None	90	1×10^{-4}
2	Penetration	40	78	None	90	1×10^{-4}
3	Cover	40	6	0.15" Circle	36	1×10^{-4}

Figure 13: CRYO-HYDROGEN TANK WELD SIMULATION

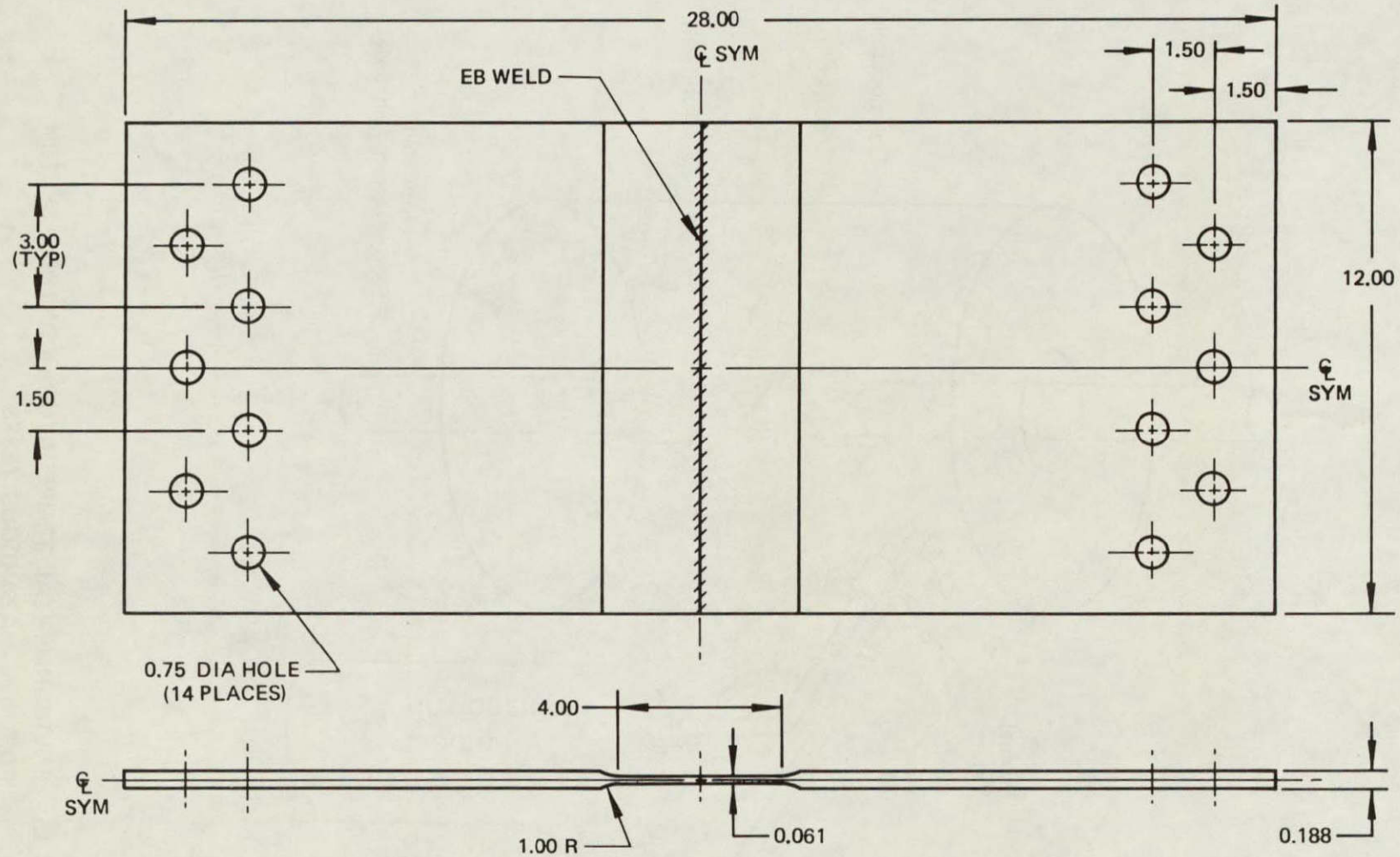

Figure 14: LACK OF PENETRATION SPECIMEN

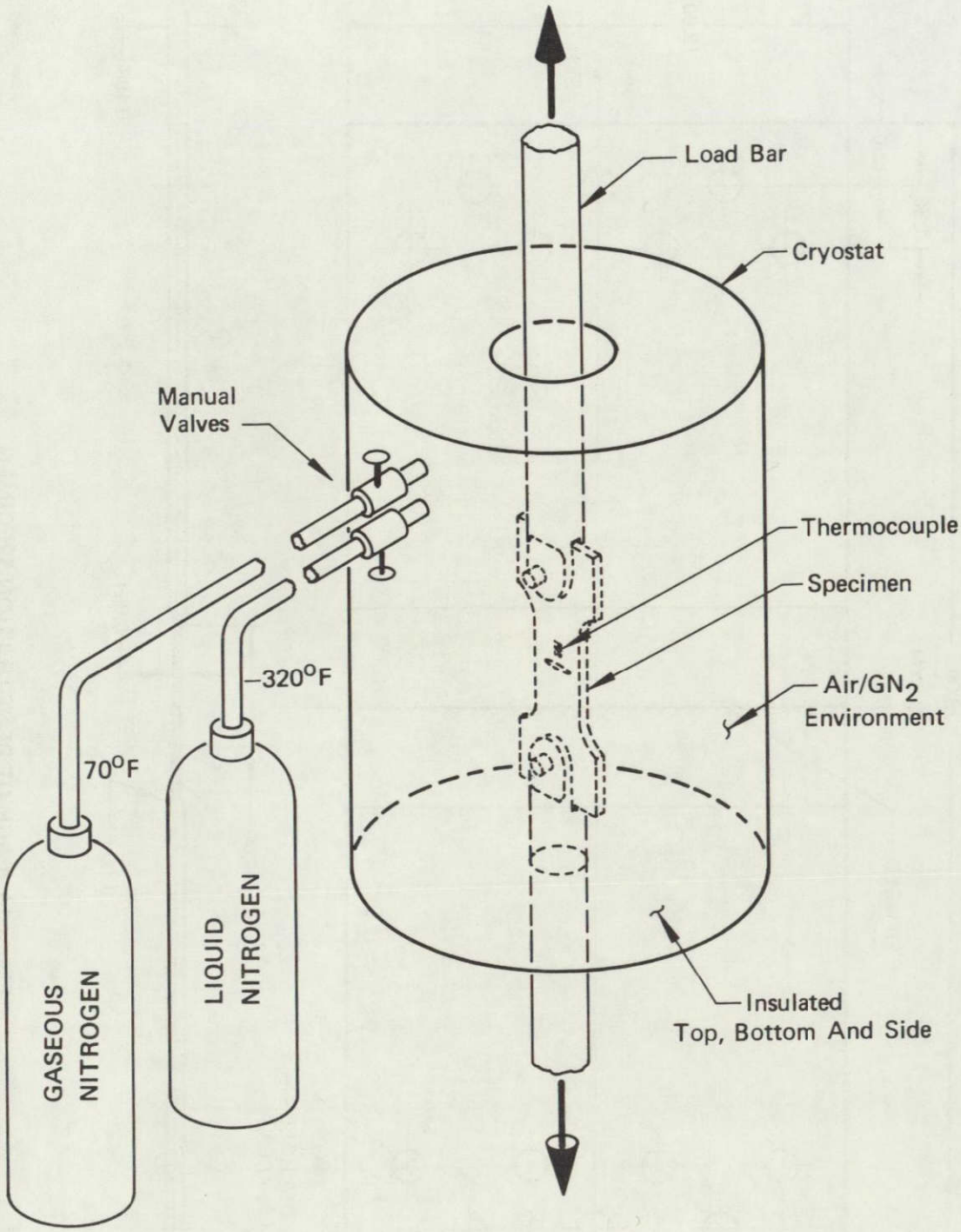

Figure 15: ENVIRONMENTAL TEMPERATURE CONTROL SYSTEM FOR NON–HAZARDOUS TESTS

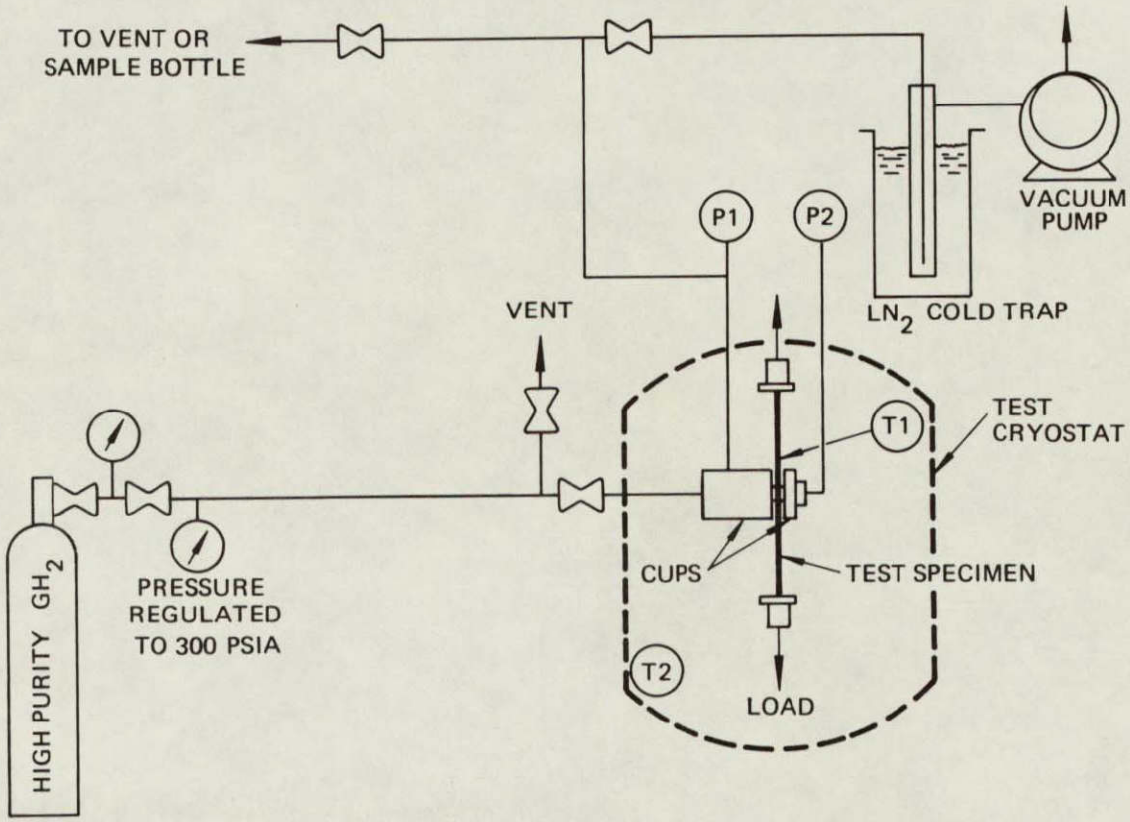

Figure 16: TEST SETUP SCHEMATIC

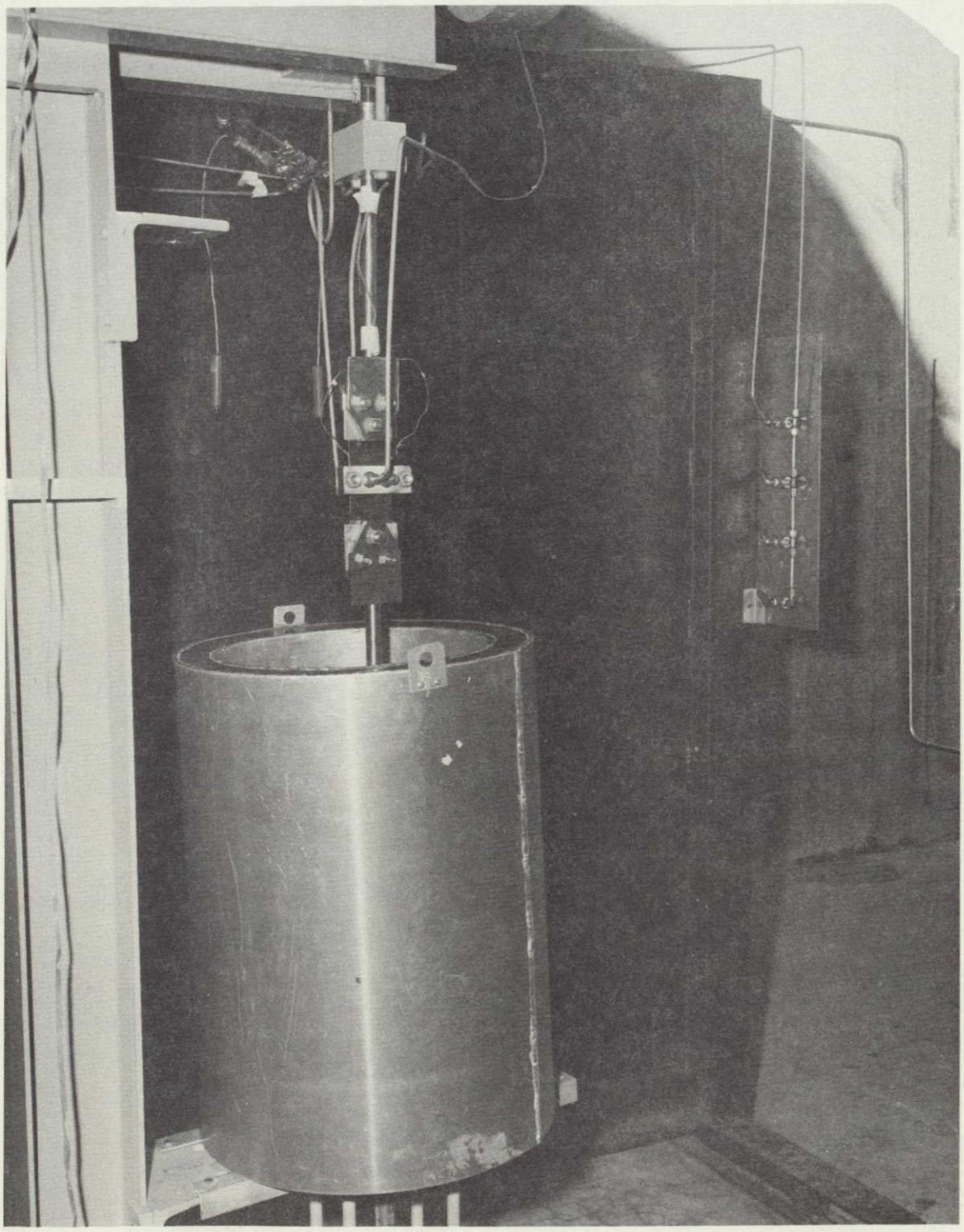

Figure 17: VIEW OF INSTALLED SPECIMEN

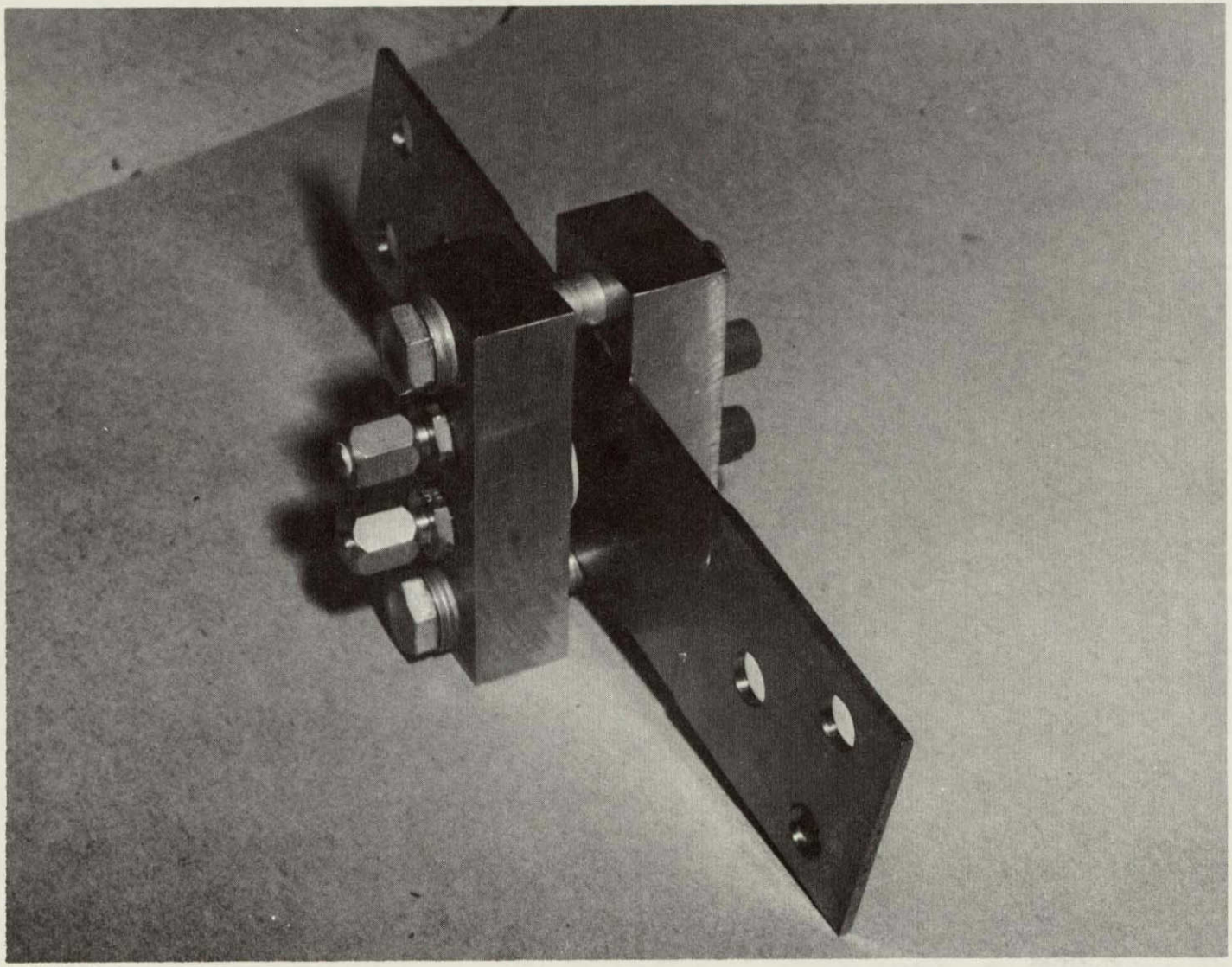

Figure 18: PRESSURE CUPS MOUNTED ON SPECIMEN

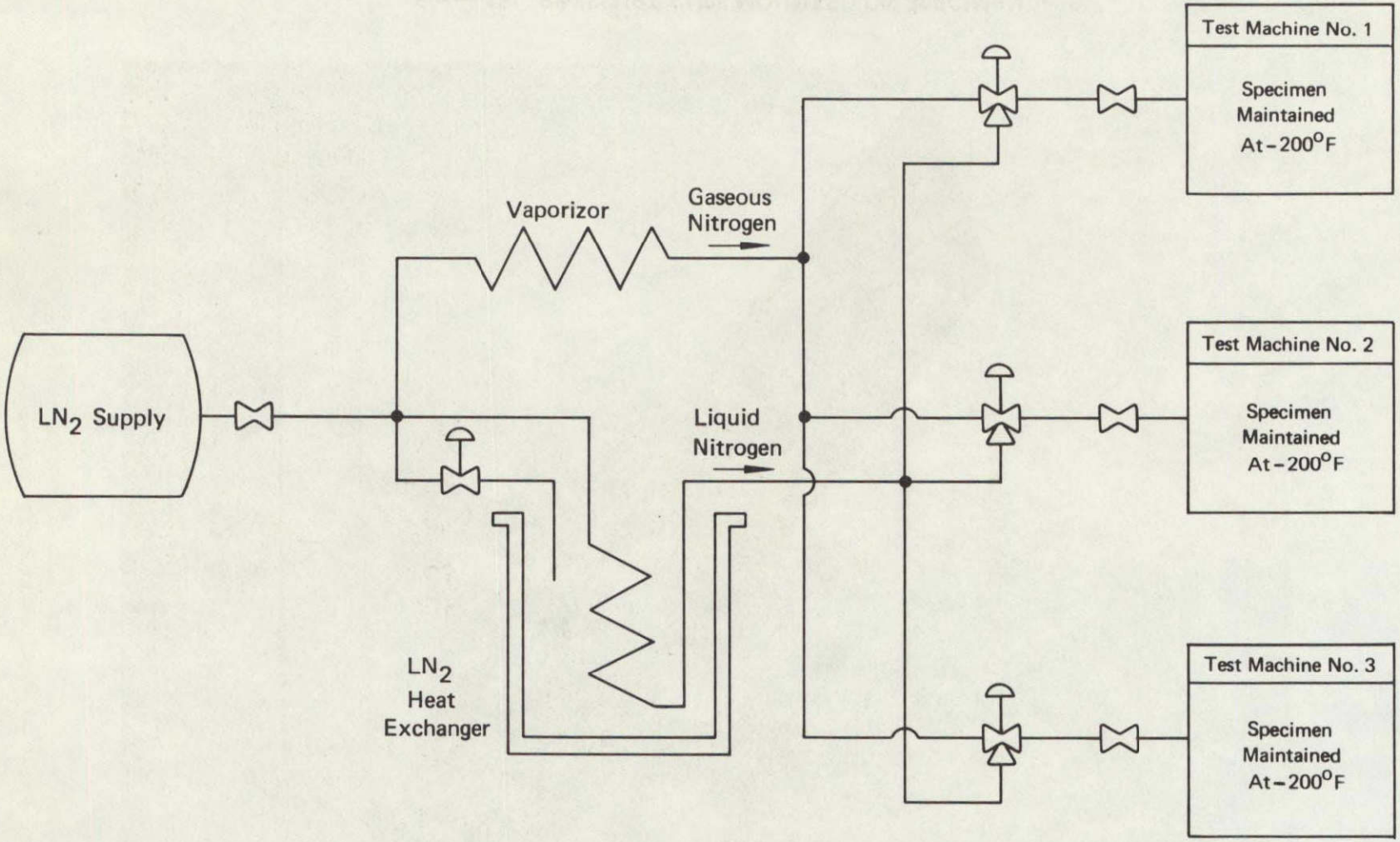

Figure 19: TEMPERATURE CONDITIONING SYSTEM FOR HAZARDOUS TESTING

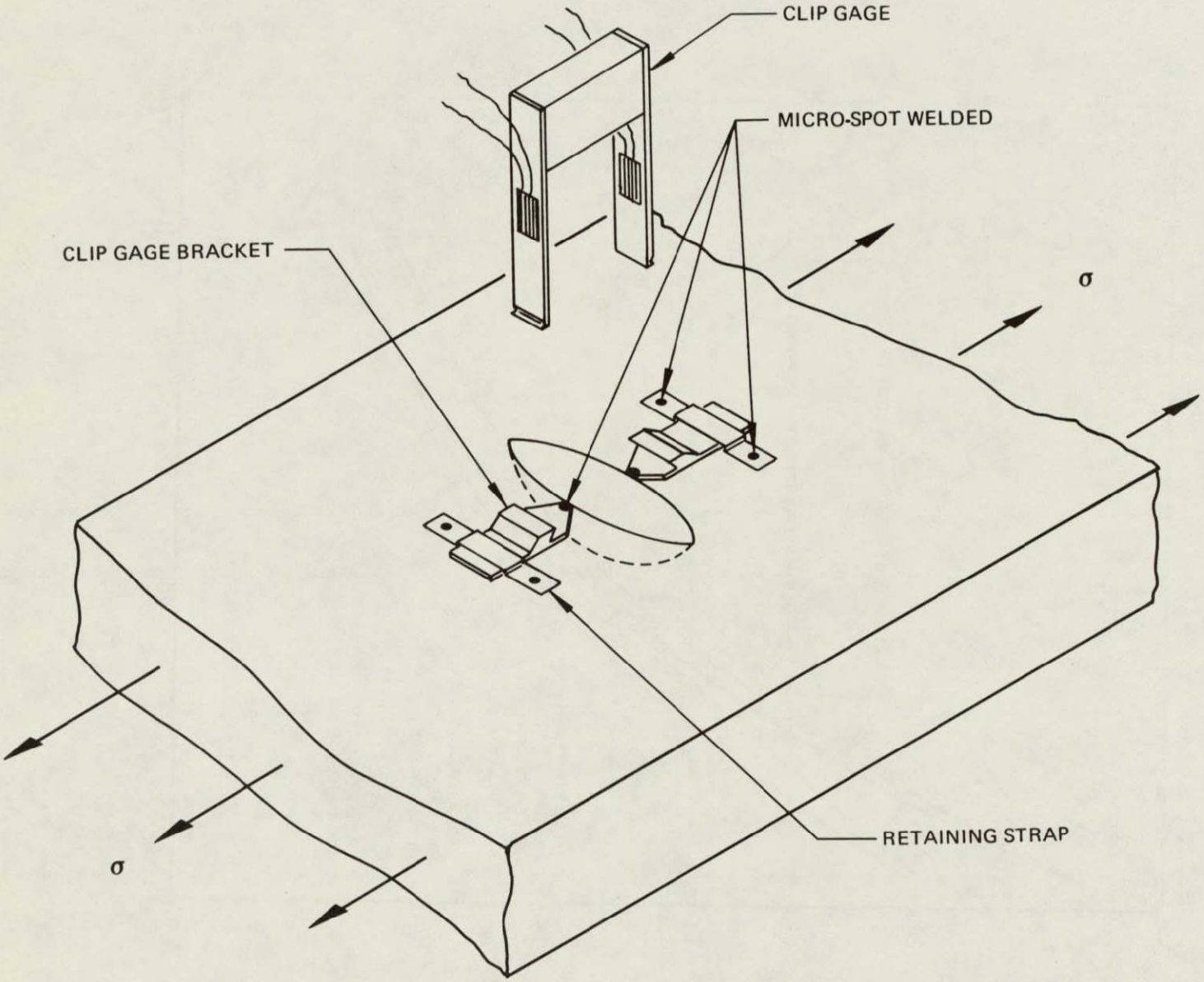

Figure 20: FLAW OPENING MEASUREMENT OF SURFACE FLAWED SPECIMENS

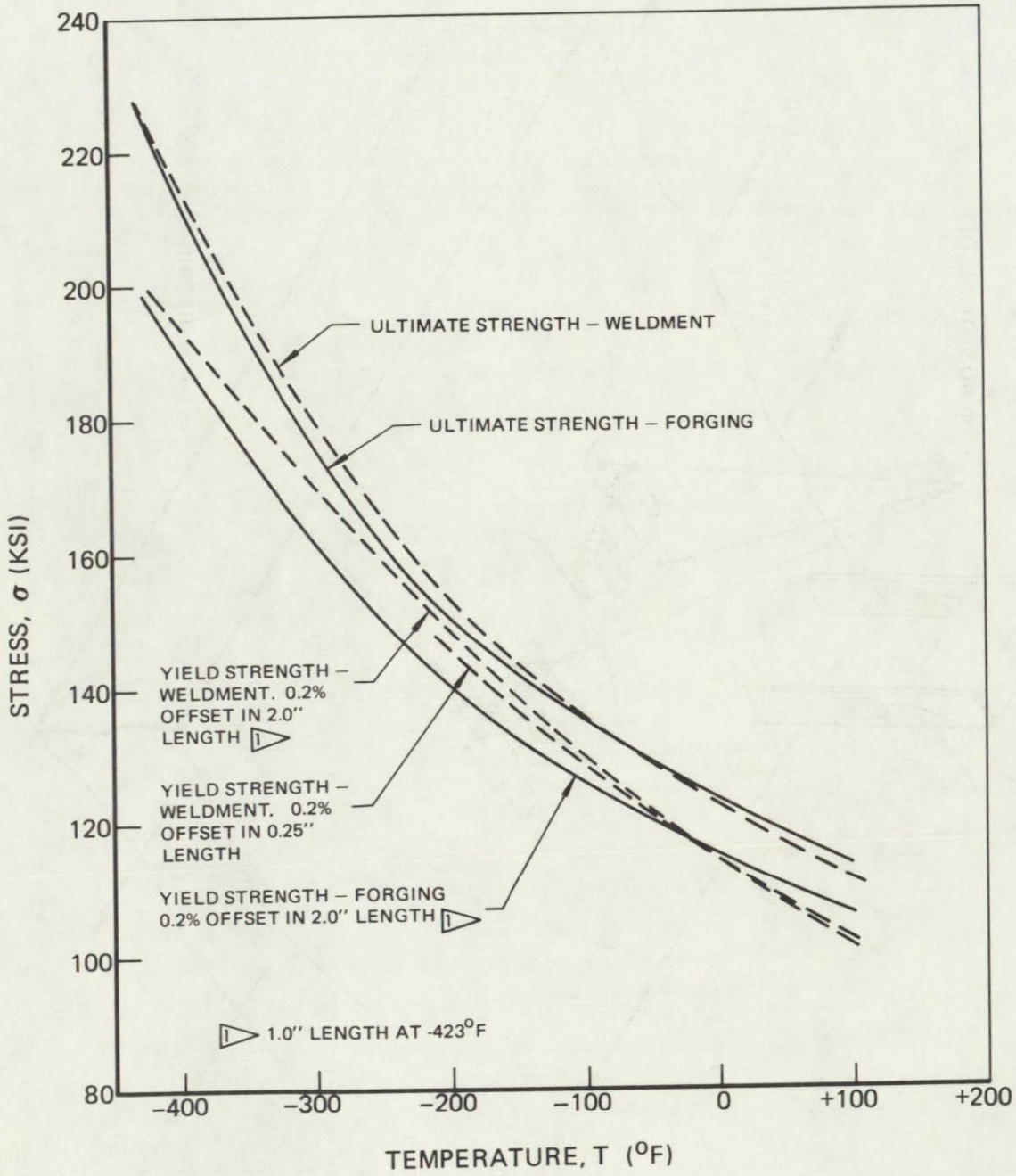

Figure 21: MECHANICAL PROPERTIES OF 5Al-2.5Sn (ELI) TITANIUM ALLOY APPLICABLE TO THE SM/EPS CRYO-HYDROGEN TANK

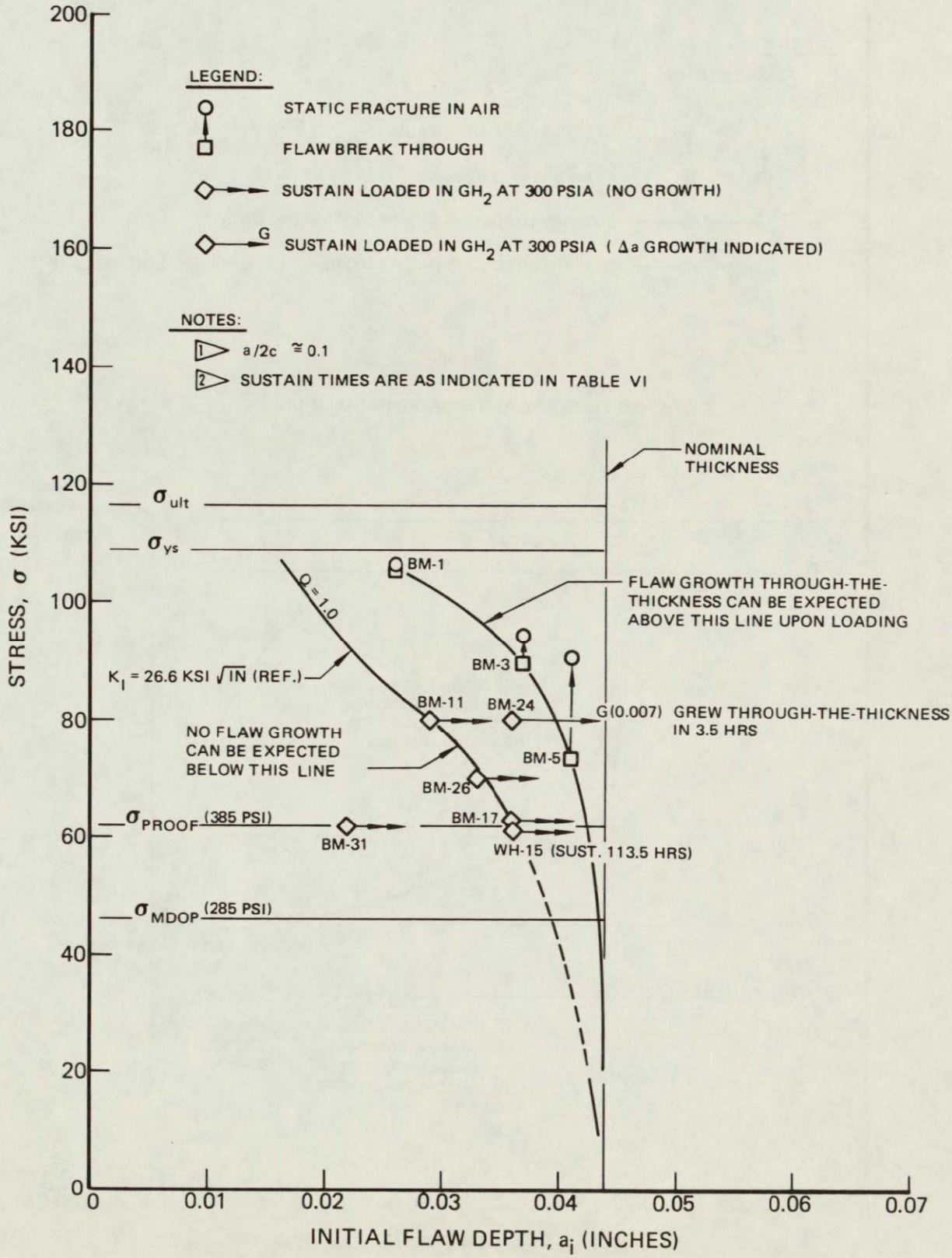

Figure 22: TEST RESULTS OF 5Al-2.5Sn (ELI) FORGING AT 70°F

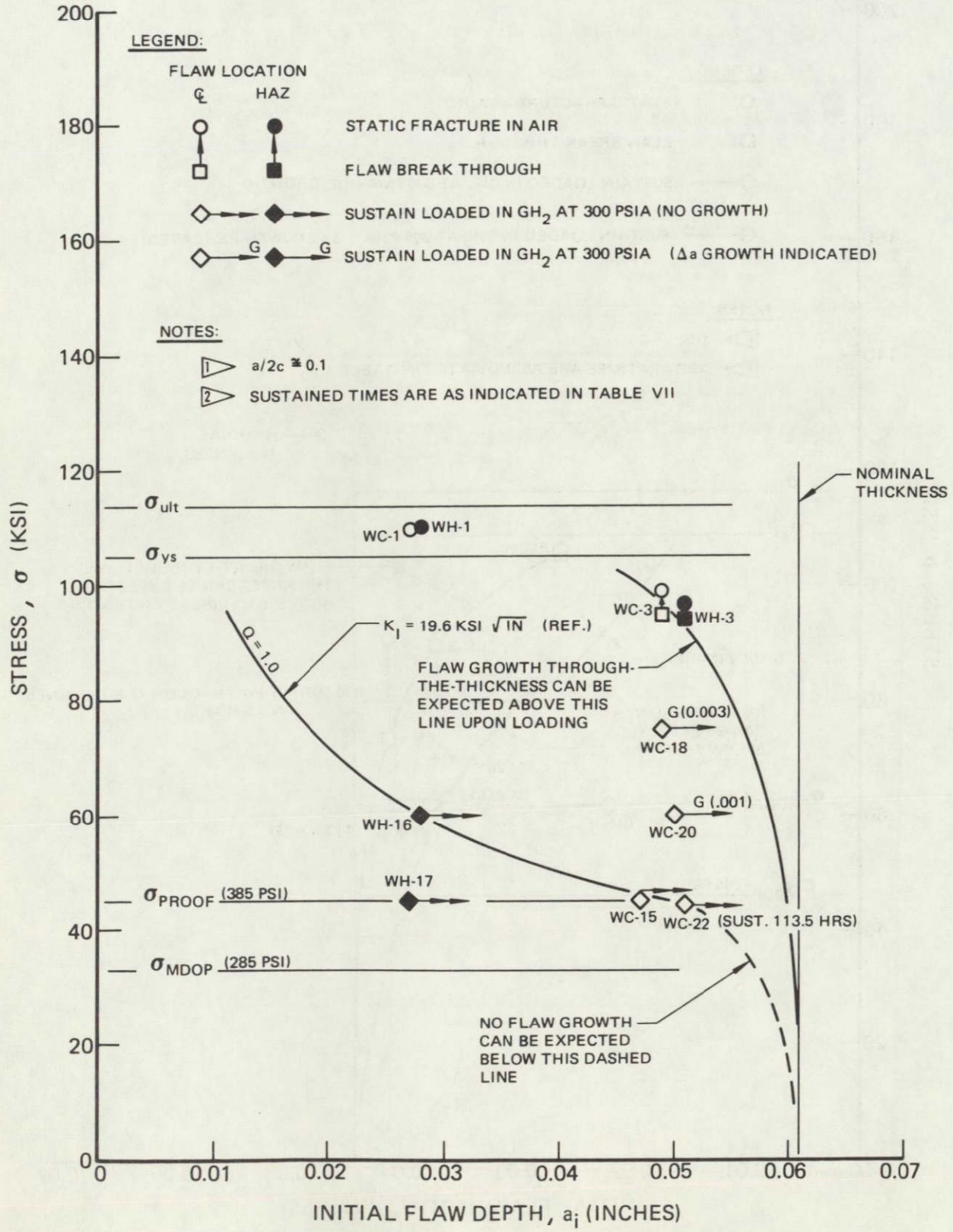

Figure 23: TEST RESULTS OF 5Al-2.5Sn (ELI) WELDMENT AT 70°F

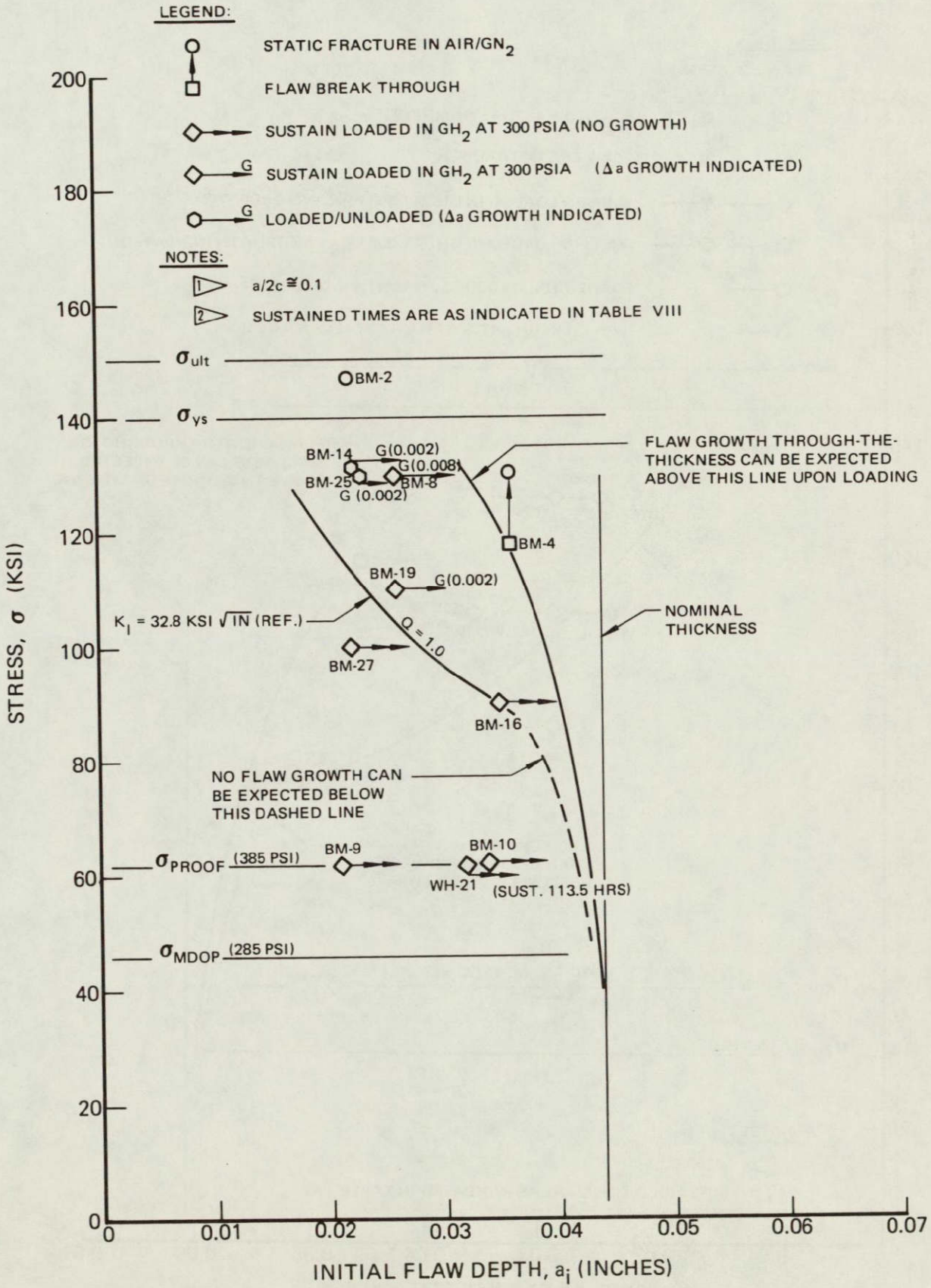

Figure 24: TEST RESULTS OF 5Al-2.5Sn (ELI) FORGING AT -200°F

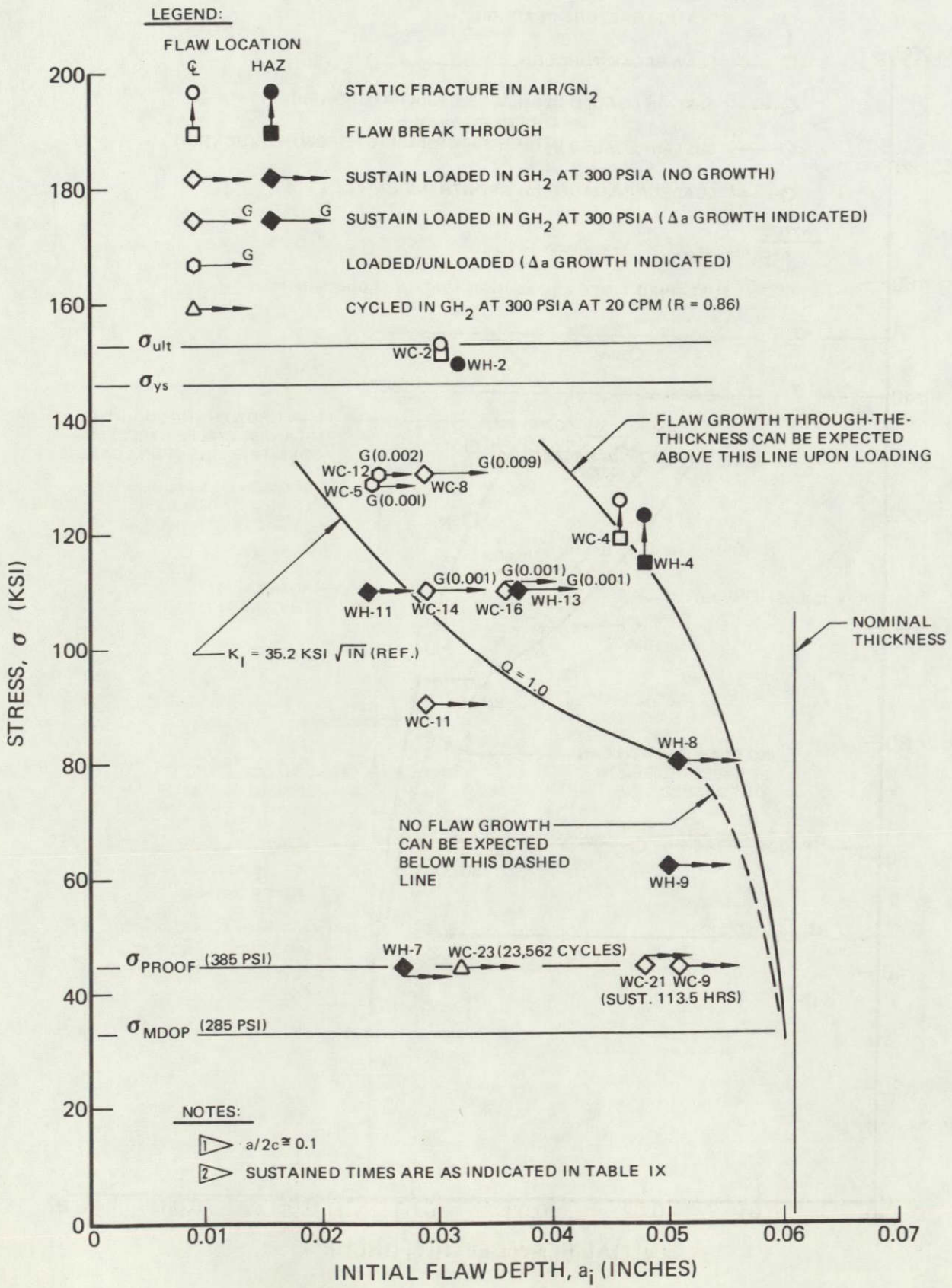

Figure 25: TEST RESULTS OF 5Al-2.5Sn (ELI) WELDMENT AT -200°F

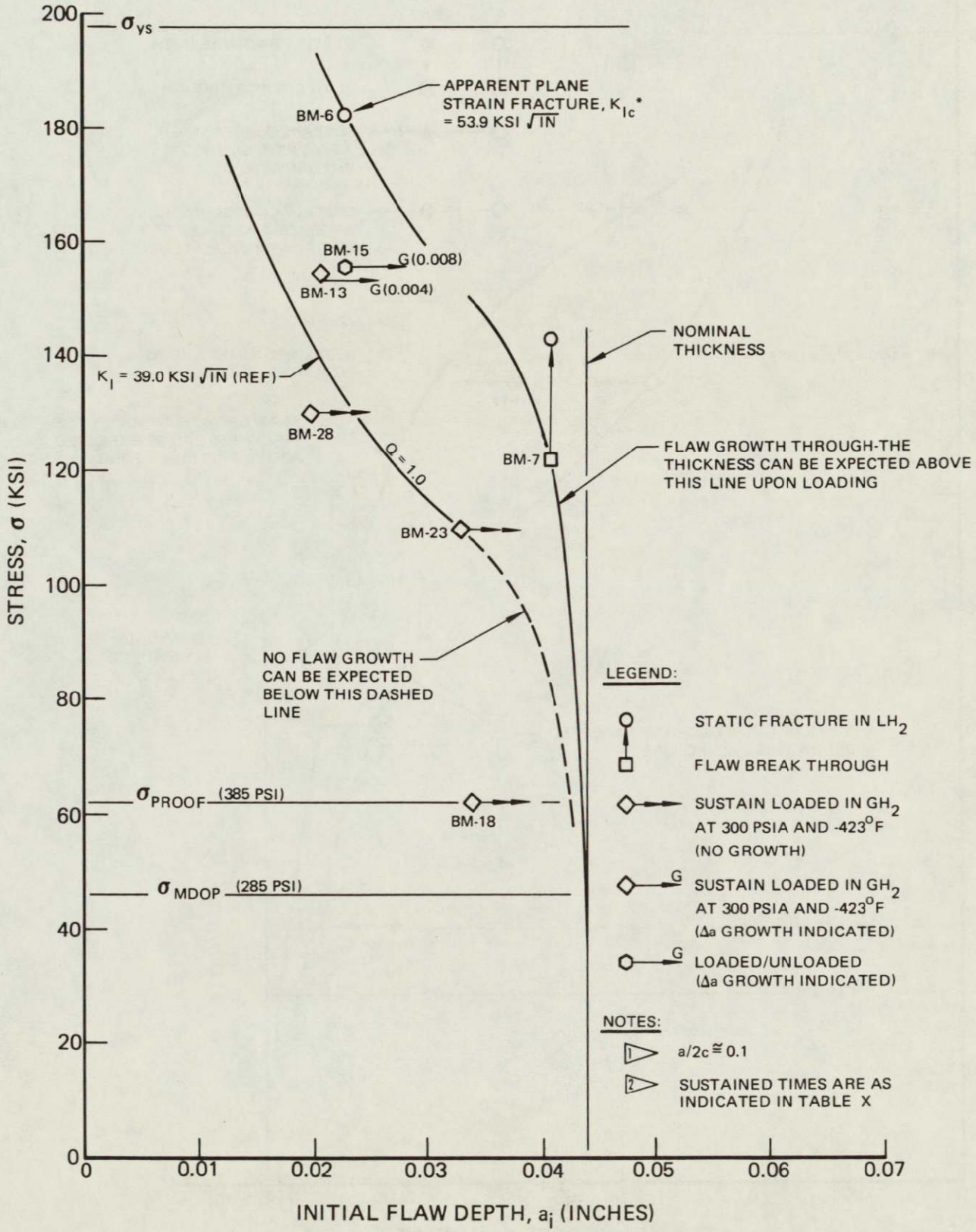

Figure 26: TEST RESULTS OF 5Al-2.5Sn (ELI) FORGING AT -423°F

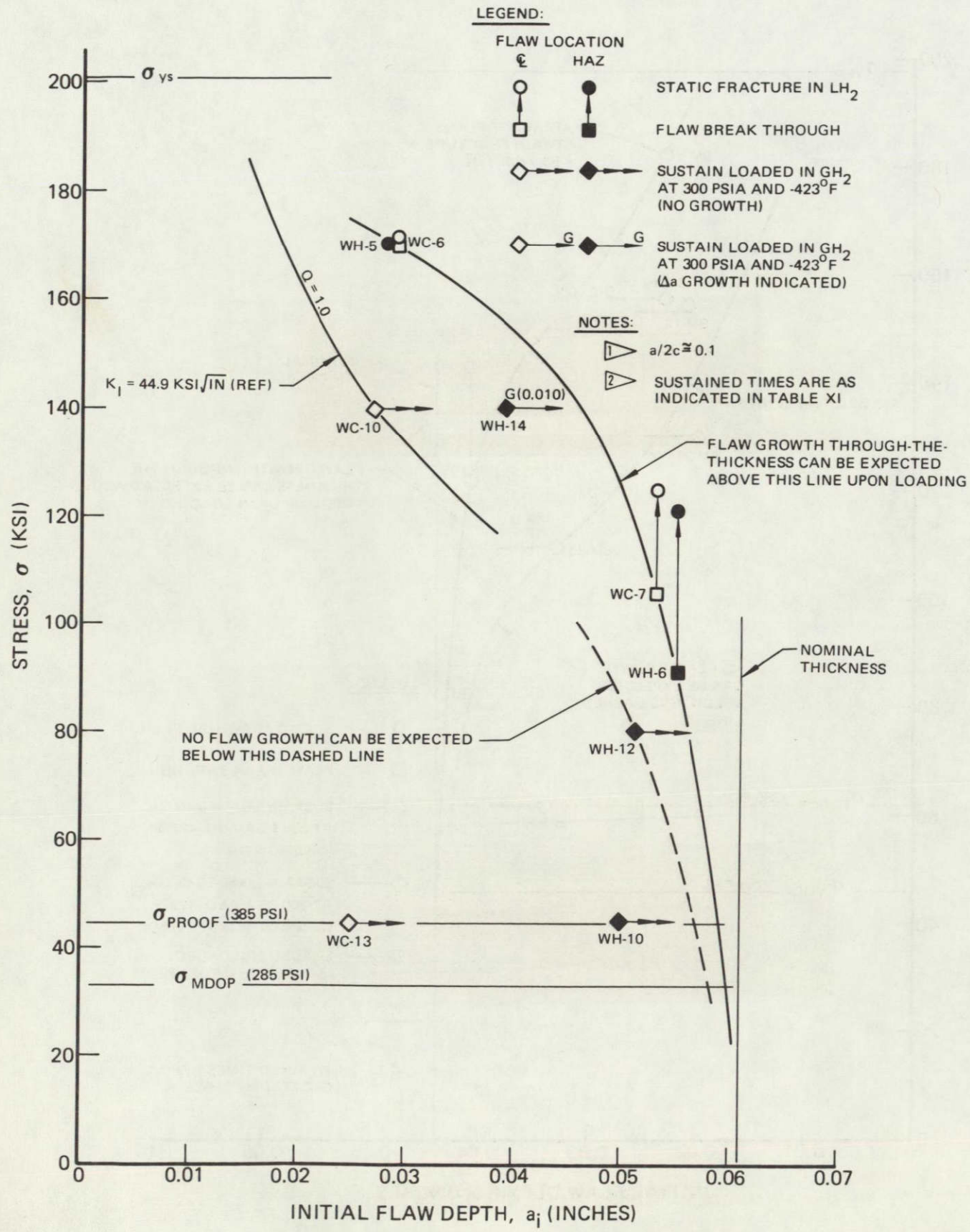

Figure 27: TEST RESULTS OF 5Al-2.5Sn (ELI) WELDMENT AT -423°F

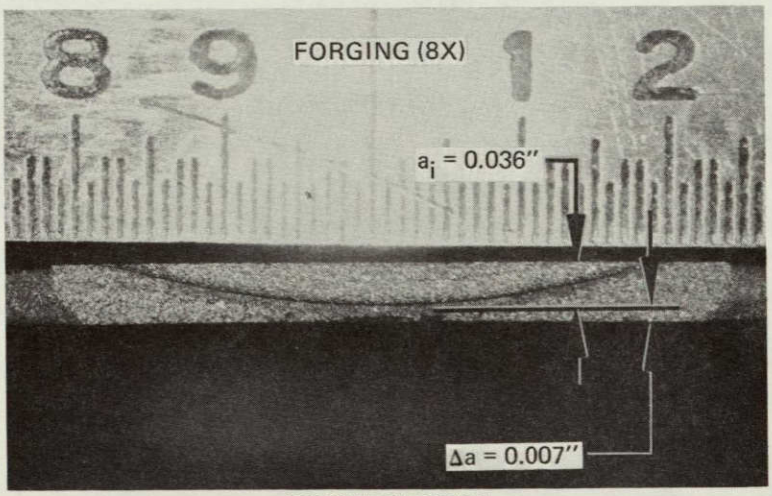

SPECIMEN BM-24
SUSTAIN LOADED,
FLAW GREW THROUGH-THE- THICKNESS IN 3.5 HRS
(σ = 80.0 Ksi)

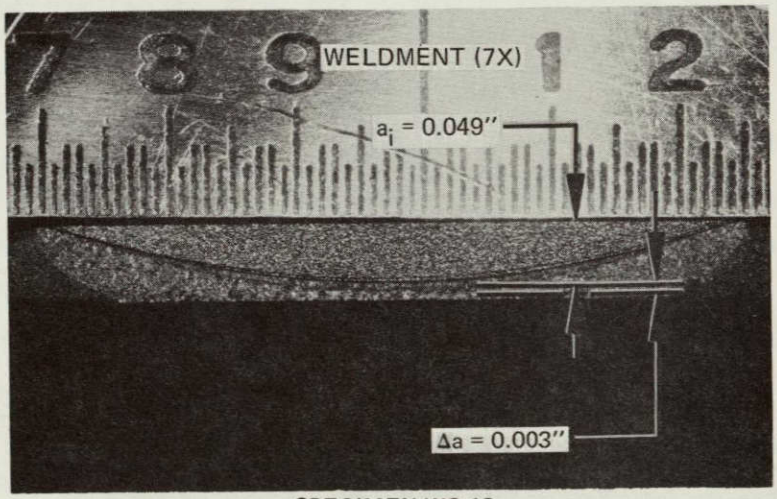

SPECIMEN WC-18
SUSTAIN LOADED FOR 20.0 HRS
(σ = 75.0 Ksi)

Figure 28 : FRACTOGRAPHS OF 5Al-2.5 Sn (ELI) TITANIUM SPECIMENS TESTED IN GH_2 AT 70°F AND 300 PSIA - POLARIZED LIGHT

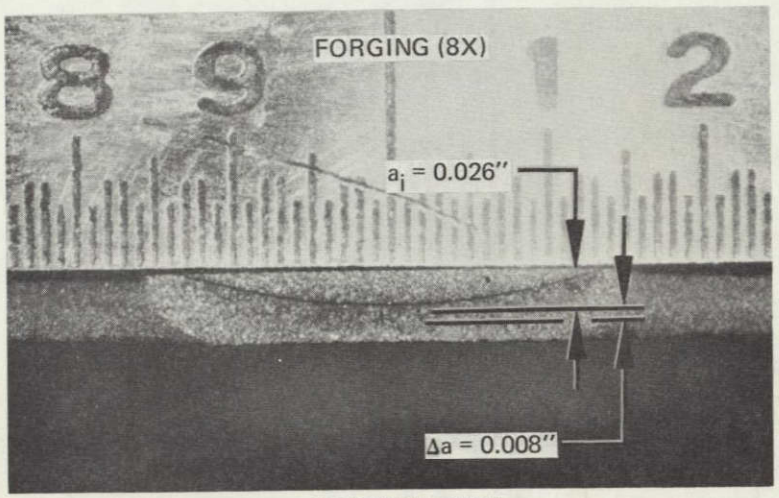

SPECIMEN BM-8
SUSTAIN LOADED FOR 20.0 HRS
(σ = 130.0 Ksi)

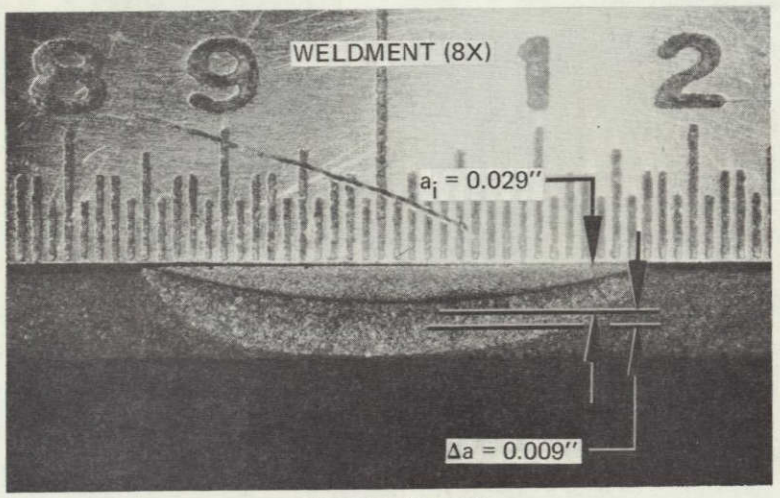

SPECIMEN WC-8
SUSTAIN LOADED FOR 20.0 HRS
(σ = 130.0 Ksi)

Figure 29 : FRACTOGRAPHS OF 5AL-2.5 Sn (ELI) TITANIUM SPECIMENS TESTED IN GH_2 AT -200°F AND 300 PSIA – POLARIZED LIGHT

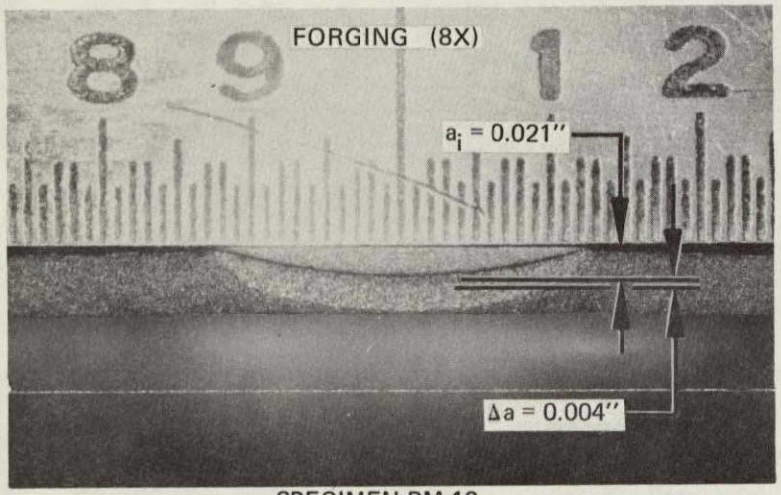

SPECIMEN BM-13
SUSTAIN LOADED FOR 15.3 HRS IN GH_2 AT 300 PSIA
(σ = 154.7 Ksi)

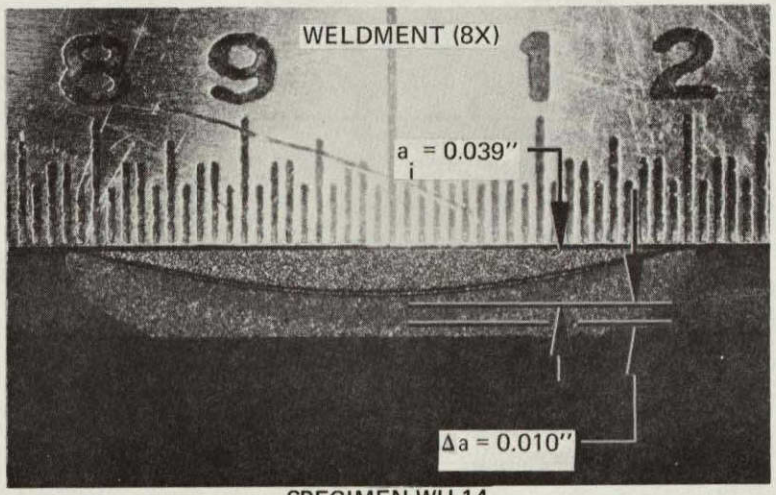

SPECIMEN WH-14
SUSTAIN LOADED FOR 20.0 HRS IN GH_2 AT 300 PSIA
(σ = 140.0 Ksi)

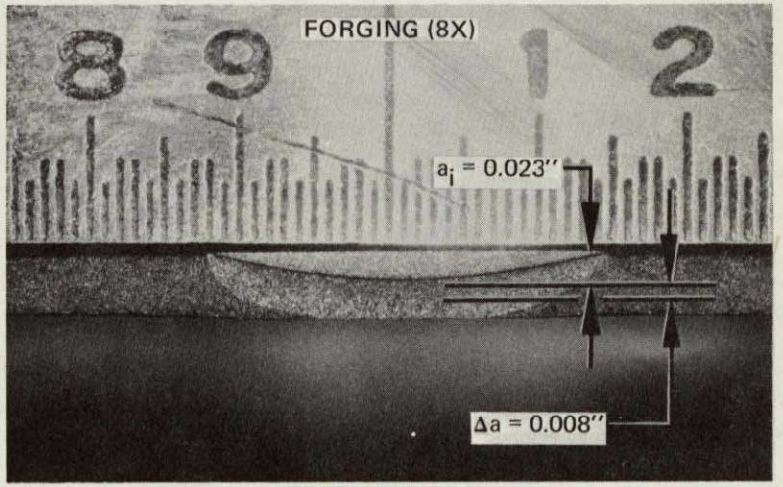

SPECIMEN BM-15
LOADED/UNLOADED IN LH_2
(σ = 154.7 Ksi)

Figure 30 : FRACTOGRAPHS OF 5AI-2.5 Sn (ELI) TITANIUM SPECIMENS TESTED IN HYDROGEN AT -423°F – POLARIZED LIGHT

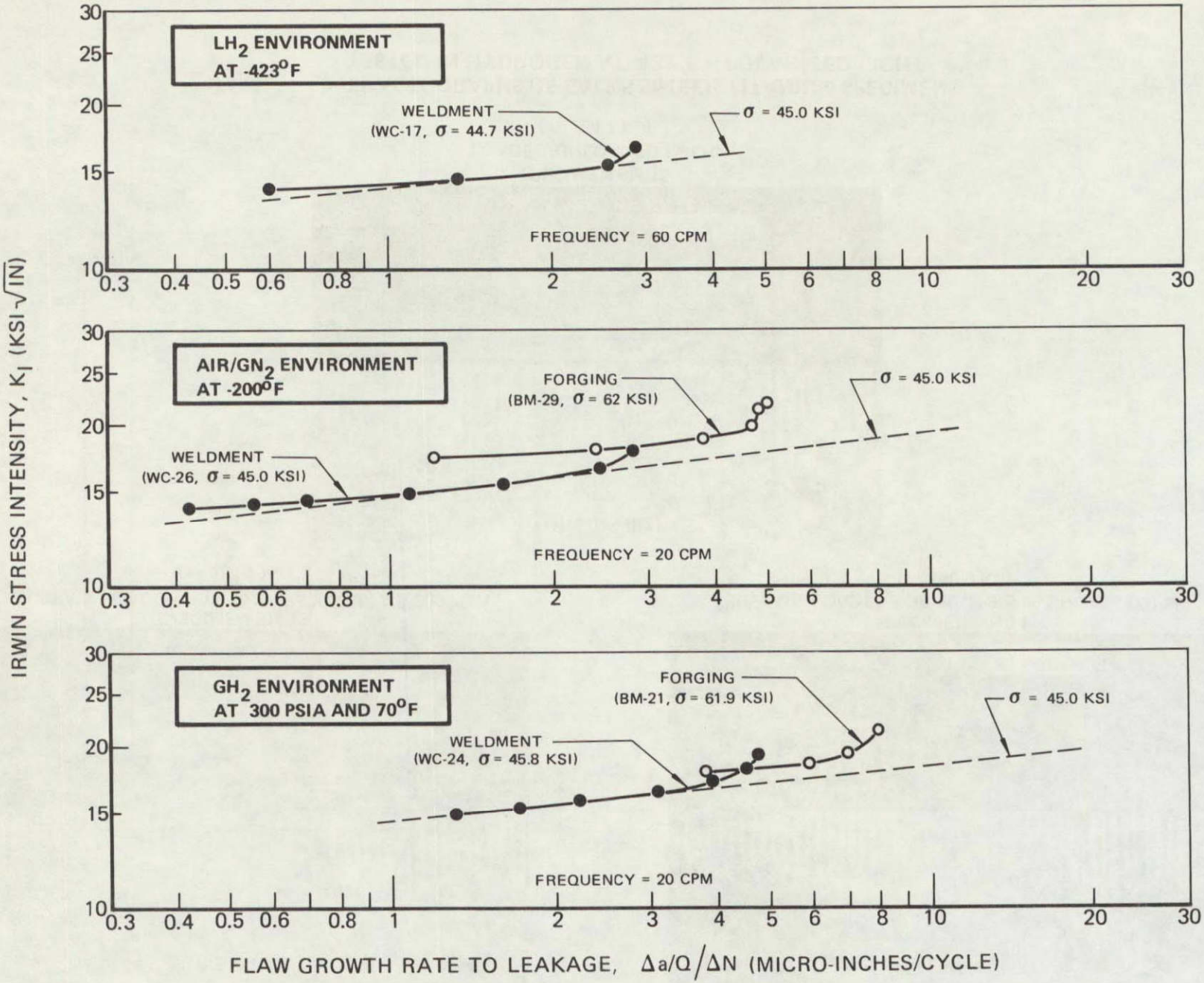

Figure 31: CYCLIC FLAW GROWTH RATES TO LEAKAGE FOR 5Al-2.5 Sn (ELI) FORGING AND WELDMENTS (R = 0.1)

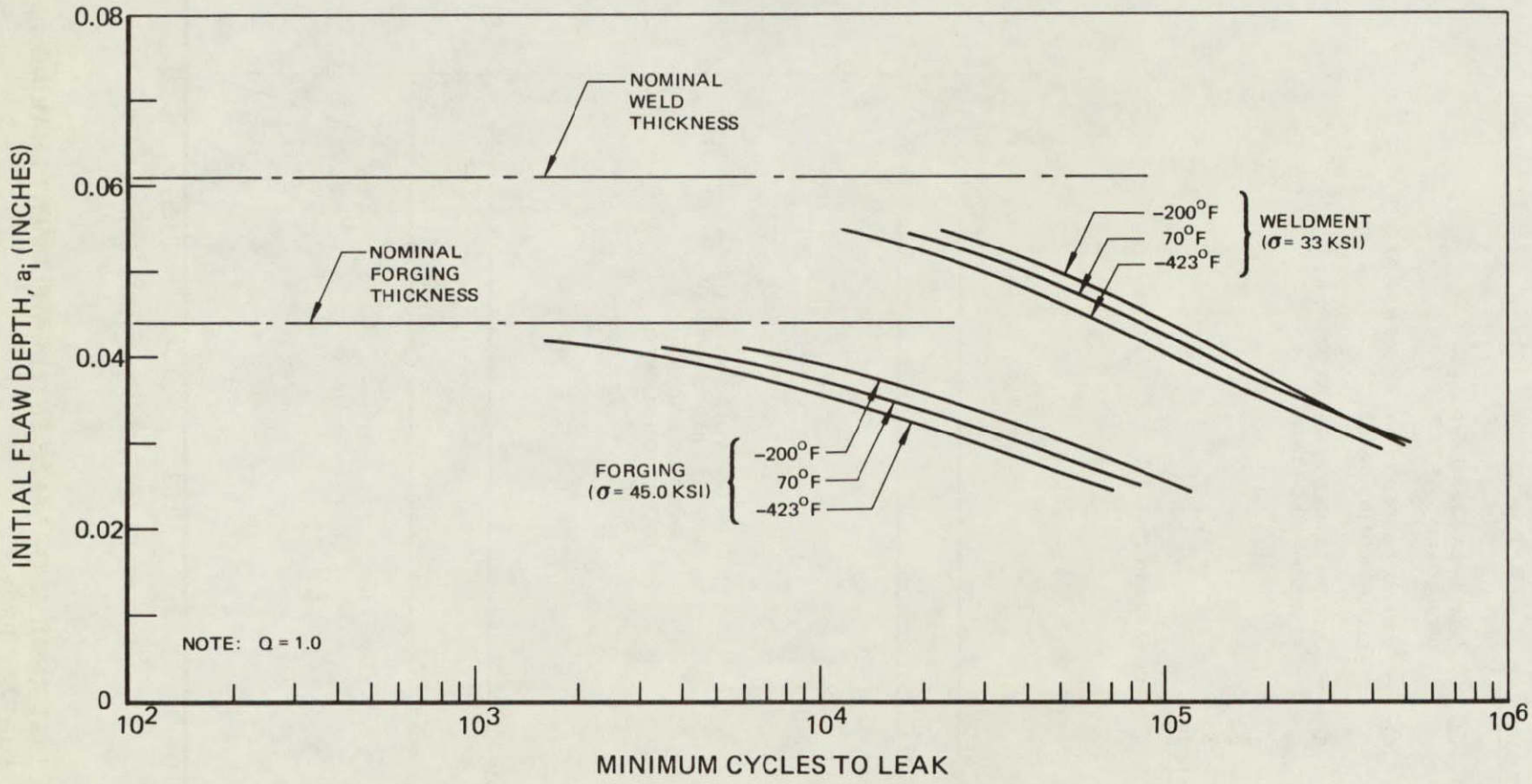

Figure 32: CYCLES TO LEAK FOR R = 0.1

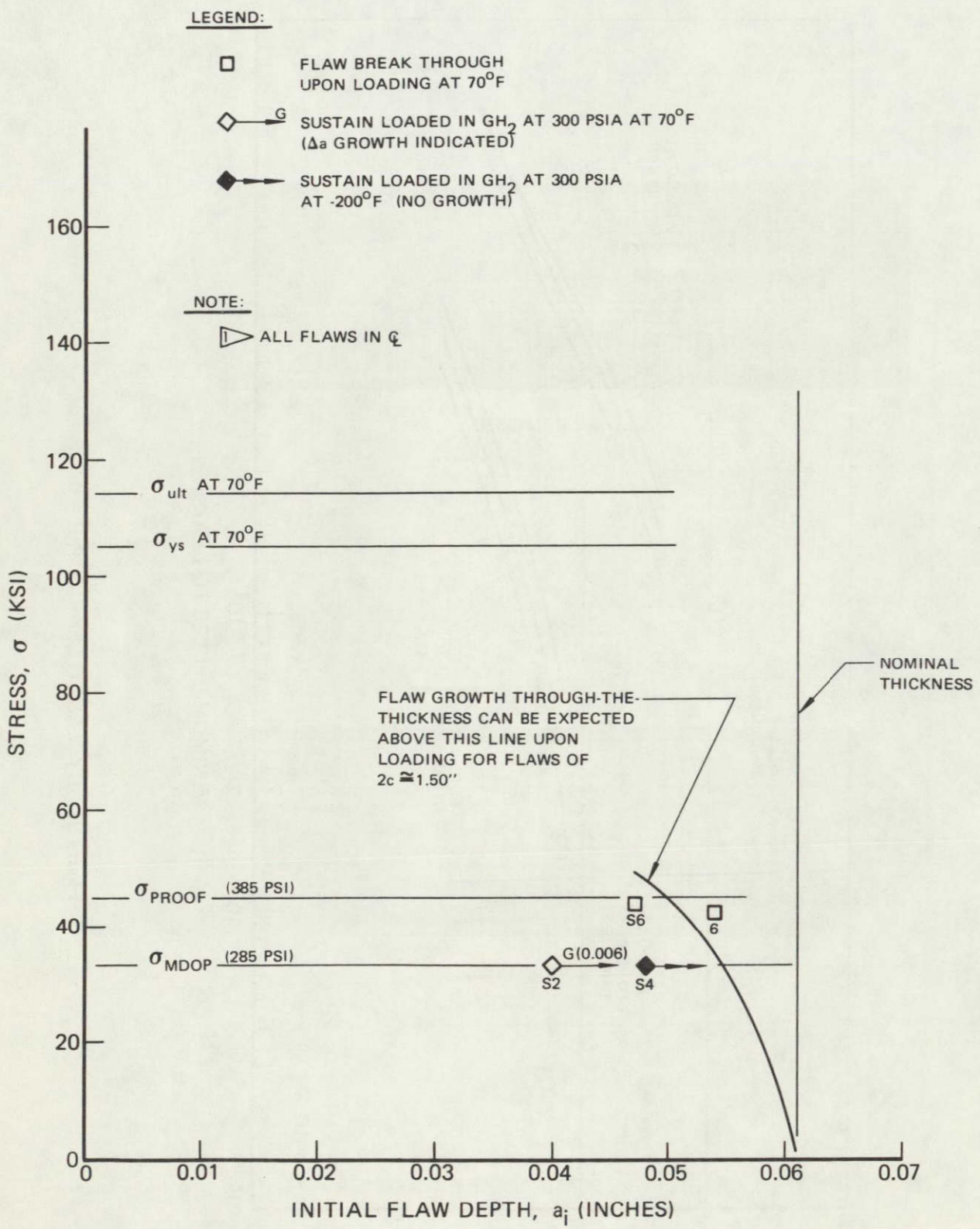

Figure 33: TEST RESULTS OF 5Al-2.5 Sn (ELI) WELDMENTS HAVING 1.5 INCH SURFACE FLAWS

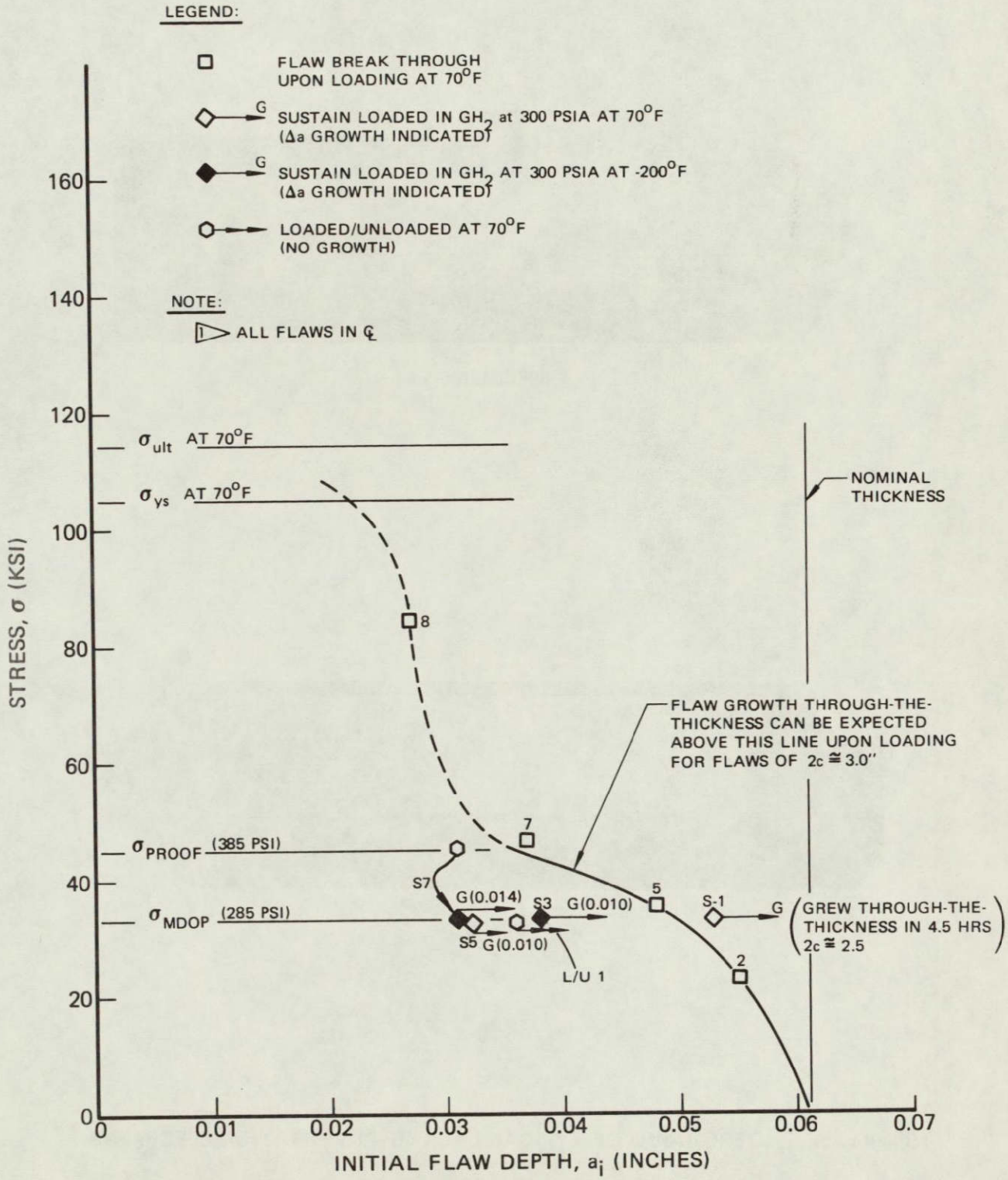

Figure 34: TEST RESULTS OF 5Al-2.5Sn (ELI) WELDMENTS HAVING 3.0 INCH SURFACE FLAWS

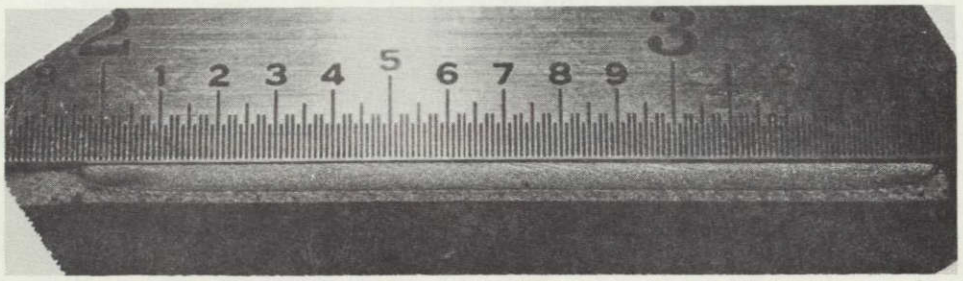

3x

SPECIMEN S-4

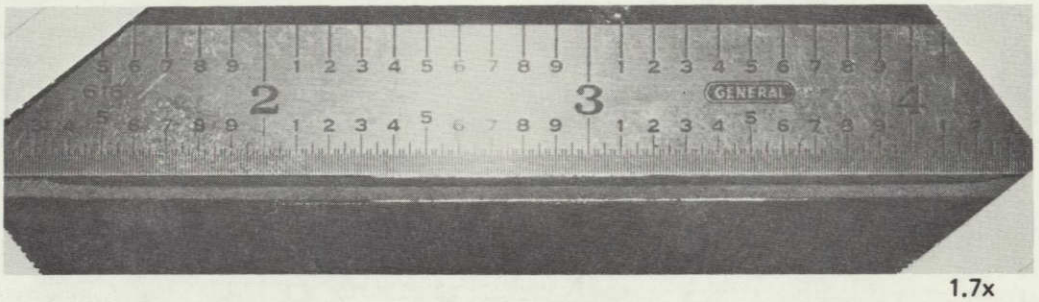

1.7x

SPECIMEN S-7

Figure 35: PHOTOGRAPHS OF TYPICAL LACK-OF-PENETRATION SPECIMENS

Table I: ANALYSIS OF HIGH PURITY GASEOUS HYDROGEN

ITEM		MSFC – SPEC -365A TABLE IA LIMITS BY VOLUME	RESULTS OF GAS ANALYSIS OBTAINED FROM AIRCO
TOTAL PURITY		99.995%	> 99.995%
IMPURITIES	NITROGEN WATER VOL. HYDRO-CARBONS	9 ppm	< 2 ppm
	OXYGEN ARGON	1 ppm	< 0.5 ppm
	HELIUM	39 ppm	< 2 ppm
	CARBON MONOXIDE AND CARBON DIOXIDE	1 ppm	< 0.5 ppm
	TOTAL IMPURITIES	50 ppm	< 5 ppm

Table II: MECHANICAL PROPERTIES OF 5Al-2.5 Sn (ELI) TITANIUM APPLICABLE TO THE SM/EPS CRYO-HYDROGEN TANK

MATERIAL	SPECIMEN NUMBER	THICKNESS, t (Inch)	WIDTH, w (Inch)	TEST ENVIRONMENT	TEST TEMPERATURE (°F)	WELD NUGGET YIELD STRENGTH 0.2% OFFSET IN 0.25 INCH LENGTH (Ksi)	YIELD STRENGTH 0.2% OFFSET IN 2.0 INCH LENGTH (Ksi)	ULTIMATE STRENGTH (Ksi)	ELONGATION % IN 2.0 INCHES
FORGING	TBM – 1	0.044	0.498	AIR	70		108.6	116.8	10
	TBM – 2	0.042	0.495	AIR	70		108.6	116.2	10
							Avg. 108.6	Avg. 116.5	Avg. 10
	TBM – 3	0.043	0.496	AIR/GN_2	-200		137.7	150.0	6
	TBM – 4	0.042	0.496	AIR/GN_2	-200		142.2	150.4	7
							Avg. 139.9	Avg. 150.2	Avg. 6
	TBM – 5	0.041	0.500	LH_2	-423		191.8 [1]	221.1	11 [1]
	TBM – 6	0.040	0.500	LH_2	-423		203.4 [1]	225.9	10 [1]
							Avg. 197.6	Avg. 223.5	Avg. 10
WELDMENT	TWC – 1	0.064	0.505	AIR	70	104.4	106.6	114.5	13
	TWH – 1	0.064	0.504	AIR	70	105.6	105.0	113.4	11
						Avg. 105.0	Avg. 105.8	Avg. 113.9	Avg. 12
	TWC – 2	0.063	0.503	AIR/GN_2	-200	149.5	151.7	155.8	6
	TWH – 2	0.063	0.504	AIR/GN_2	-200	142.2	146.0	149.8	8
						Avg. 145.8	Avg. 148.8	Avg. 152.8	Avg. 7
	TWC – 3	0.063	0.492	LH_2	-423	NOT OBTAINED	207.1 [1]	231.6	9 [1]
	TWH – 3	0.063	0.489	LH_2	-423		195.2 [1]	217.5	11 [1]
							Avg. 201.1	Avg. 224.5	Avg. 10

[1] 1.0 INCH GAGE LENGTH

Table III: STATIC FRACTURE TESTS OF 5Al-2.5 Sn (ELI) TITANIUM TESTED AT 70°F IN AIR

MATERIAL	SPECIMEN NUMBER	FLAW LOCATION	THICKNESS, t (Inch)	WIDTH, w (Inch)	INITIAL FLAW DEPTH, a_i (Inch)	INITIAL FLAW LENGTH, $2c_i$ (Inch)	$(a/2c)_i$	GROSS STRESS AT FLAW BREAKTHROUGH, σ_T (Ksi)	GROSS STRESS AT FAILURE, σ_F (Ksi)	YIELD STRENGTH, σ_{ys} (Ksi)	σ_T / σ_{ys}	σ_F / σ_{ys}	a_i / t
FORGING	BM-1	–	0.045	1.598	0.026	0.270	0.0963	105.4	106.1	108.6	0.971	0.977	0.578
	BM-3	–	0.044	1.596	0.037	0.395	0.0937	89.2	94.0		0.821	0.865	0.841
	BM-5	–	0.045	1.589	0.041	0.440	0.0932	73.6	90.5	108.6	0.678	0.833	0.911
WELDMENT	WC-1	℄	0.061	2.496	0.027	0.295	0.0915	110.1	110.1	105.0	1.049	1.049	0.443
	WC-3	℄	0.062	2.495	0.049	0.530	0.0925	95.0	98.3		0.905	0.936	0.790
	WH-1	HAZ	0.059	2.497	0.028	0.290	0.0966	110.6	110.6		1.054	1.054	0.475
	WH-3	HAZ	0.062	2.512	0.051	0.540	0.0945	94.4	96.3	105.0	0.899	0.917	0.823

Table IV: STATIC FRACTURE TESTS OF 5Al-25 Sn (ELI) TITANIUM TESTED AT -200°F IN AIR/GASEOUS NITROGEN

MATERIAL	SPECIMEN NUMBER	FLAW LOCATION	THICKNESS, t (Inch)	WIDTH, w (Inch)	INITIAL FLAW DEPTH, a_i (Inch)	INITIAL FLAW LENGTH, $2c_i$ (Inch)	$(a/2c)_i$	GROSS STRESS AT FLAW BREAKTHROUGH, σ_T (Ksi)	GROSS STRESS AT FAILURE, σ_F (Ksi)	YIELD STRENGTH, σ_{ys} (Ksi)	σ_T / σ_{ys}	σ_F / σ_{ys}	a_i / t
FORGING	BM-2	–	0.044	1.597	0.022	0.260	0.0846	147.1	147.1	139.9	1.051	1.051	0.500
	BM-4	–	0.045	1.598	0.036	0.385	0.0935	117.9	130.3	139.9	0.843	0.932	0.800
WELDMENT	WC-2	℄	0.063	2.495	0.031	0.305	0.1000	141.0	153.0	145.8	1.036	1.049	0.492
	WC-4	℄	0.061	2.497	0.046	0.520	0.0885	118.8	125.4		0.815	0.860	0.754
	WH-2	HAZ	0.060	2.496	0.032	0.310	0.1032	149.8	149.8		1.028	1.028	0.533
	WH-4	HAZ	0.062	2.510	0.048	0.545	0.0881	114.6	128.0	145.8	0.786	0.878	0.774

Table V: STATIC FRACTURE TESTS OF 5Al-2.5 Sn (ELI) TITANIUM TESTED AT -423°F IN LIQUID HYDROGEN

MATERIAL	SPECIMEN NUMBER	FLAW LOCATION	THICKNESS, t (Inch)	WIDTH, w (Inch)	INITIAL FLAW DEPTH, a_i (Inch)	INITIAL FLAW LENGTH, $2c_i$ (Inch)	$(a/2c)_i$	GROSS STRESS AT FLAW BREAKTHROUGH, σ_T (Ksi)	GROSS STRESS AT FAILURE, σ_F (Ksi)	YIELD STRENGTH, σ_{ys} (Ksi)	σ_T / σ_{ys}	σ_F / σ_{ys}	a_i / t	
FORGING	BM-6	–	0.045	1.591	0.023	0.255	0.0902	182.0	182.0	197.6	0.921	0.921	0.511	1
	BM-7	–	0.046	1.599	0.041	0.405	0.1012	121.8	142.9	197.6	0.616	0.723	0.891	
WELDMENT	WC-6	℄	0.060	2.502	0.029	0.335	0.0866	169.7	171.7	201.1	0.844	0.854	0.484	
	WC-7	℄	0.061	2.501	0.053	0.545	0.0973	105.6	124.9		0.525	0.621	0.868	
	WH-5	HAZ	0.059	2.493	0.028	0.340	0.0824	170.2	170.2		0.847	0.847	0.474	
	WH-6	HAZ	0.061	2.493	0.055	0.550	0.1000	91.0	121.0	201.1	0.453	0.602	0.902	

1 APPARENT PLANE STRAIN FRACTURE, K^*_{Ic} = 53.9 KSI$\sqrt{IN}$

Table VI: SUSTAINED TESTS OF 5AI-2.5 Sn (ELI) TITANIUM FORGING TESTED AT 70°F IN GASEOUS HYDROGEN AT 300 PSIA

SPECIMEN NUMBER	THICKNESS, t (Inch)	WIDTH, w (Inch)	INITIAL FLAW DEPTH, a_i (Inch)	INITIAL FLAW LENGTH, $2c_i$ (Inch)	$(a/2c)_i$	APPLIED GROSS STRESS, σ_A (Ksi)	YIELD STRENGTH, σ_{ys} (Ksi)	σ_A / σ_{ys}	a_i / t	SUSTAINED TIME (Hours)	OBSERVATIONS
BM-11	0.045	1.598	0.029	0.285	0.1017	80.0	108.6	0.737	0.645	14.0	NO GROWTH
BM-17	0.046	1.596	0.036	0.402	0.0895	62.0		0.571	0.783	20.0	NO GROWTH
BM-24	0.043	1.597	0.036	0.383	0.0914	80.0		0.737	0.837	3.5	GROWTH THROUGH-THE-THICKNESS
BM-26	0.044	1.592	0.033	0.380	0.0869	70.0		0.645	0.750	20.0	NO GROWTH
BM-31	0.044	1.593	0.022	0.257	0.0856	62.0		0.571	0.500	20.0	NO GROWTH
WH-15	0.044	2.503	0.036	0.388	0.0928	61.9	108.6	0.570	0.819	113.5	NO GROWTH

Table VIIa: SUSTAINED TESTS OF 5Al-2.5 Sn (ELI) TITANIUM WELDMENT TESTED AT 70°F IN GASEOUS HYDROGEN AT 300 PSIA (FLAWS IN ℄)

SPECIMEN NUMBER	THICKNESS, t (Inch)	WIDTH, w (Inch)	INITIAL FLAW DEPTH, a_i (Inch)	INITIAL FLAW LENGTH, $2c_i$ (Inch)	$(a/2c)_i$	APPLIED GROSS STRESS, σ_A (Ksi)	YIELD STRENGTH, σ_{ys} (Ksi)	σ_A / σ_{ys}	a_i / t	SUSTAINED TIME (Hours)	OBSERVATIONS
WC-15	0.061	2.501	0.047	0.533	0.0882	45.0	105.0	0.428	0.771	20.0	NO GROWTH
WC-18	0.060	2.501	0.049	0.530	0.0925	75.0		0.714	0.816	20.0	GROWTH (Δa = 0.002")
WC-20	0.061	2.504	0.050	0.533	0.0948	60.0		0.571	0.820	20.0	GROWTH (Δa = 0.001")
WC-22	0.062	2.501	0.051	0.562	0.0908	43.9	105.0	0.418	0.823	113.5	NO GROWTH

Table VIIb: SUSTAINED TESTS OF 5Al-2.5 Sn (ELI) TITANIUM WELDMENT TESTED AT 70°F IN GASEOUS HYDROGEN AT 300 PSIA (FLAWS IN HAZ)

SPECIMEN NUMBER	THICKNESS, t (Inch)	WIDTH, w (Inch)	INITIAL FLAW DEPTH, a_i (Inch)	INITIAL FLAW LENGTH, $2c_i$ (Inch)	$(a/2c)_i$	APPLIED GROSS STRESS, σ_A (Ksi)	YIELD STRENGTH, σ_{ys} (Ksi)	σ_A / σ_{ys}	a_i / t	SUSTAINED TIME (Hours)	OBSERVATIONS
WH-16	0.062	2.500	0.028	0.302	0.0927	60.0	105.0	0.571	0.452	20.0	NO GROWTH
WH-17	0.061	2.501	0.027	0.298	0.0906	45.0	105.0	0.428	0.443	20.0	NO GROWTH

Table VIII: SUSTAINED TESTS OF 5Al-2.5 Sn (ELI) TITANIUM FORGING TESTED AT -200°F IN GASEOUS HYDROGEN AT 300 PSIA

SPECIMEN NUMBER	THICKNESS, t (Inch)	WIDTH, w (Inch)	INITIAL FLAW DEPTH, a_i (Inch)	INITIAL FLAW LENGTH, $2c_i$ (Inch)	$(a/2c)_i$	APPLIED GROSS STRESS, σ_A (Ksi)	YIELD STRENGTH, σ_{ys} (Ksi)	σ_A / σ_{ys}	a_i / t	SUSTAINED TIME (Hours)	OBSERVATIONS
BM-8	0.046	1.602	0.026	0.272	0.0956	130.0	139.9	0.929	0.565	20.0	GROWTH (Δa = 0.008")
BM-9	0.047	1.600	0.021	0.245	0.0857	62.0		0.443	0.447	20.0	NO GROWTH
BM-10	0.047	1.598	0.034	0.420	0.0810	62.0		0.443	0.724	14.0	NO GROWTH
BM-16	0.045	1.601	0.035	0.397	0.0882	90.0		0.644	0.778	20.0	NO GROWTH
BM-19	0.047	1.597	0.026	0.260	0.1000	110.0		0.786	0.554	20.0	GROWTH (Δa = 0.002")
BM-27	0.044	1.598	0.022	0.256	0.0860	100.0		0.715	0.500	20.0	NO GROWTH
WH-21	0.045	2.503	0.032	0.385	0.0831	61.9	139.9	0.443	0.711	113.5	NO GROWTH

Table IXa: SUSTAINED TESTS OF 5Al-2.5 Sn (ELI) TITANIUM WELDMENT TESTED AT -200°F IN GASEOUS HYDROGEN AT 300 PSIA (FLAWS IN ℄)

SPECIMEN NUMBER	THICKNESS, t (Inch)	WIDTH, w (Inch)	INITIAL FLAW DEPTH, a_i (Inch)	INITIAL FLAW LENGTH, $2c_i$ (Inch)	$(a/2c)_i$	APPLIED GROSS STRESS, σ_A (Ksi)	YIELD STRENGTH, σ_{ys} (Ksi)	σ_A / σ_{ys}	a_i / t	SUSTAINED TIME (Hours)	OBSERVATIONS
WC-8	0.060	2.492	0.029	0.320	0.0907	130.0	145.8	0.892	0.484	20.0	GROWTH (Δa = 0.009")
WC-9	0.061	2.491	0.051	0.555	0.0917	45.0		0.309	0.836	13.0	NO GROWTH
WC-11	0.061	2.501	0.029	0.310	0.0936	90.0		0.617	0.475	13.5	NO GROWTH
WC-14	0.063	2.503	0.029	0.310	0.0936	109.9		0.754	0.461	18.0	GROWTH (Δa = 0.001")
WC-16	0.061	2.502	0.036	0.397	0.0907	110.0		0.755	0.591	20.0	GROWTH (Δa = 0.001")
WC-21	0.063	2.502	0.048	0.532	0.0902	44.8	145.8	0.307	0.762	113.5	NO GROWTH

Table IXb: SUSTAINED TESTS OF 5Al-2.5 Sn (ELI) TITANIUM WELDMENT TESTED AT -200°F IN GASEOUS HYDROGEN AT 300 PSIA (FLAWS IN HAZ)

SPECIMEN NUMBER	THICKNESS, t (Inch)	WIDTH, w (Inch)	INITIAL FLAW DEPTH, a_i (Inch)	INITIAL FLAW LENGTH, $2c_i$ (Inch)	$(a/2c)_i$	APPLIED GROSS STRESS, σ_A (Ksi)	YIELD STRENGTH, σ_{ys} (Ksi)	σ_A / σ_{ys}	a_i / t	SUSTAINED TIME (Hours)	OBSERVATIONS
WH-7	0.061	2.493	0.027	0.305	0.0885	45.0	145.8	0.309	0.442	20.0	NO GROWTH
WH-8	0.061	2.500	0.051	0.565	0.0903	80.0		0.549	0.836	13.0	NO GROWTH
WH-9	0.059	2.496	0.050	0.560	0.0893	62.0		0.425	0.847	13.5	NO GROWTH
WH-11	0.061	2.503	0.024	0.290	0.0828	109.9		0.754	0.394	18.0	NO GROWTH
WH-13	0.063	2.498	0.037	0.400	0.0925	110.0	145.8	0.755	0.588	20.0	GROWTH (Δa = 0.001")

Table X: SUSTAINED TESTS OF 5Al-2.5 Sn (ELI) TITANIUM FORGING TESTED AT -423°F IN GASEOUS HYDROGEN AT 300 PSIA

SPECIMEN NUMBER	THICKNESS, t (Inch)	WIDTH, w (Inch)	INITIAL FLAW DEPTH, a_i (Inch)	INITIAL FLAW LENGTH, $2c_i$ (Inch)	$(a/2c)_i$	APPLIED GROSS STRESS, σ_A (Ksi)	YIELD STRENGTH, σ_{ys} (Ksi)	σ_A / σ_{ys}	a_i / t	SUSTAINED TIME (Hours)	OBSERVATIONS
BM-13	0.045	1.598	0.021	0.250	0.0840	154.7	197.6	0.783	0.467	15.3	GROWTH (Δa = 0.004")
BM-18	0.046	1.597	0.034	0.402	0.0846	62.0		0.314	0.740	20.0	NO GROWTH
BM-23	0.043	1.599	0.033	0.385	0.0857	110.0		0.557	0.767	20.0	NO GROWTH
BM-28	0.044	1.598	0.020	0.246	0.0813	130.0	197.6	0.658	0.454	20.0	NO GROWTH

Table XIa: SUSTAINED TESTS OF 5AI-2.5 Sn (ELI) TITANIUM WELDMENT TESTED AT -423°F IN GASEOUS HYDROGEN AT 300 PSIA (FLAWS IN ℄)

SPECIMEN NUMBER	THICKNESS, t (Inch)	WIDTH, w (Inch)	INITIAL FLAW DEPTH, a_i (Inch)	INITIAL FLAW LENGTH, $2c_i$ (Inch)	$(a/2c)_i$	APPLIED GROSS STRESS, σ_A (Ksi)	YIELD STRENGTH, σ_{ys} (Ksi)	σ_A / σ_{ys}	a_i / t	SUSTAINED TIME (Hours)	OBSERVATIONS
WC-10	0.062	2.492	0.027	0.310	0.0871	140.0	201.1	0.696	0.436	16.0	NO GROWTH
WC-13	0.061	2.502	0.025	0.290	0.0862	45.0	201.1	0.224	0.410	20.0	NO GROWTH

Table XIb: SUSTAINED TESTS OF 5AI-2.5 Sn (ELI) TITANIUM WELDMENT TESTED AT -423°F IN GASEOUS HYDROGEN AT 300 PSIA (FLAWS IN HAZ)

SPECIMEN NUMBER	THICKNESS, t (Inch)	WIDTH, w (Inch)	INITIAL FLAW DEPTH, a_i (Inch)	INITIAL FLAW LENGTH, $2c_i$ (Inch)	$(a/2c)_i$	APPLIED GROSS STRESS, σ_A (Ksi)	YIELD STRENGTH, σ_{ys} (Ksi)	σ_A / σ_{ys}	a_i / t	SUSTAINED TIME (Hours)	OBSERVATIONS
WH-10	0.061	2.505	0.050	0.550	0.0909	45.0	201.1	0.224	0.820	16.0	NO GROWTH
WH-12	0.061	2.503	0.051	0.553	0.0922	80.0		0.398	0.836	20.0	NO GROWTH
WH-14	0.061	2.498	0.039	0.410	0.0951	140.0	201.1	0.696	0.639	20.0	GROWTH (Δa = 0.010")

Table XII: LOAD/UNLOAD TESTS OF 5Al-2.5 Sn (ELI) TITANIUM

MATERIAL	SPECIMEN NUMBER	FLAW LOCATION	THICKNESS, t (Inch)	WIDTH, w (Inch)	INITIAL FLAW DEPTH, a_i (Inch)	INITIAL FLAW LENGTH, $2c_i$ (Inch)	$(a/2c)_i$	APPLIED GROSS STRESS, σ_A (Ksi)	YIELD STRENGTH, σ_{ys} (Ksi)	σ_A / σ_{ys}	a_i/t	TEST ENVIRONMENT	TEST TEMPERATURE (^oF)	OBSERVATIONS
FORGING	BM-14	—	0.046	1.598	0.023	0.255	0.0902	130.0	139.9	0.930	0.500	GN_2	-200	GROWTH (Δa = 0.002")
	BM-15	—	0.046	1.599	0.023	0.260	0.0885	154.7	197.6	0.783	0.500	LH_2	-423	GROWTH (Δa = 0.008")
	BM-25	—	0.043	1.600	0.023	0.250	0.0920	130.0	139.9	0.930	0.535	GH_2	-200	GROWTH (Δa = 0.002")
WELDMENT	WC-5	℄	0.063	2.505	0.025	0.298	0.0840	130.0	145.8	0.892	0.397	GN_2	-200	GROWTH (Δa = 0.001")
	WC-12	℄	0.063	2.503	0.025	0.303	0.0825	130.0	145.8	0.892	0.397	GH_2	-200	GROWTH (Δa = 0.002")

Table XIII: CYCLIC FLAW GROWTH RATES OF 5Al-2.5 Sn (ELI) TITANIUM FORGING

SPECIMEN NUMBER [1]	THICKNESS, t (Inch)	TEST CONDITIONS AT	FLAW DEPTH, a (Inch)	FLAW WIDTH, 2c (Inch)	a/2c	STRESS, σ (Ksi)	σ/σ_{ys}	STRESS RATIO, R	FLAW SIZE, (a/Q) (Inch)	a/t	STRESS INTENSITY, K_I (Ksi $\sqrt{in}$)	(K_I) Avg. (Ksi$\sqrt{in}$)	$(\Delta(a/Q)/\Delta N)$ Avg. (micro-inch/cycle)	ENVIRONMENT	TEMPERATURE (^oF)	OBSERVATIONS
BM-21	0.042	Initiation	0.022	0.250	0.088	61.9	0.57	0.10	0.022	0.524	17.8	20.3	6.89	GH_2 AT 300 PSIA	70	Grew through-the-thickness in 2,033 cycles at 20 CPM
		Termination	0.042	0.250	0.168				0.036	1.0	22.8					
BM-20	0.046	Initiation	0.024	0.235	0.102	45.8	0.33	0.10	0.022	0.522	13.3	13.4	0.04	GH_2 AT 300 PSIA	-200	Δa = 0.001 growth in 26,190 cycles at 20 CPM
		Termination	0.025	0.235	0.106				0.023	0.543	13.5					
BM-29	0.044	Initiation	0.021	0.243	0.086	62.0	0.44	0.10	0.020	0.477	17.2	20.0	3.77	AIR/ GN_2	-200	Grew through-the-thickness in 4,250 cycles at 20 CPM
		Termination	0.044	0.243	0.181				0.036	1.0	22.8					
BM-30	0.043	Initiaton	0.023	0.245	0.094	62.0	0.44	0.86	0.022	0.535	17.9	17.9	0	AIR/ GN_2	-200	No growth in 83,400 cycles at 60 CPM
		Termination	0.023	0.245	0.094				0.022	0.535	17.9					
BM-22	0.044	Initiation	0.025	0.245	0.102	61.9	0.31	0.10	0.023	0.568	18.3	20.5	3.83	LH_2	-423	Grew through-the-thickness in 3,136 cycles at 60 CPM [2]
		Termination	0.044	0.245	0.180				0.035	1.0	22.7					

[1] ALL SPECIMENS 1.6" WIDE

[2] INSTRUMENTATION OUTPUT IN ERROR, FLAW OPENING DECREASED INSTEAD OF INCREASING, REASON UNKNOWN

Table XIV: CYCLIC FLAW GROWTH RATES OF 5Al-2.5 Sn (ELI) TITANIUM WELDMENT (FLAWS IN ℄)

SPECIMEN NUMBER △	THICKNESS, t (Inch)	TEST CONDITIONS AT	FLAW DEPTH, a (Inch)	FLAW WIDTH, 2c (Inch)	a/2c	STRESS, σ (Ksi)	σ/σ_{ys}	STRESS RATIO, R	FLAW SIZE, (a/Q) (Inch)	a/t	STRESS INTENSITY, K_I (Ksi $\sqrt{in}$)	$(K_I)_{Avg.}$ (Ksi $\sqrt{in}$)	$(\Delta(a/Q)/\Delta N)_{Avg.}$ (micro-inch/cycle)	ENVIRONMENT	TEMPERATURE (°F)	OBSERVATIONS
WC-24	0.062	Initiation	0.028	0.318	0.088	45.8	0.44	0.10	0.027	0.452	14.7	17.2	3.11	GH_2 AT 300 PSIA	70	Grew through-the thickness in 7,065 cycles at 20 CPM
		Termination	0.062	0.318	0.195				0.049	1.0	19.7					
WC-25	0.064	Initiation	0.028	0.295	0.095	33.0	0.23	0.10	0.026	0.438	10.4	10.4	0	AIR/ GN_2	-200	No growth in 12,300 cycles at 20 CPM
		Termination	0.028	0.295	0.095				0.026	0.438	10.4					
WC-26	0.065	Initiation	0.026	0.300	0.087	45.0	0.31	0.10	0.025	0.400	13.8	16.5	1.49	AIR/ GN_2	-200	Grew through-the-thickness in 15,392 cycles at 20 CPM
		Termination	0.065	0.300	0.217				0.048	1.0	19.3					
WC-23	0.063	Initiation	0.032	0.312	0.103	45.8	0.31	0.86	0.030	0.508	15.4	15.4	0	GH_2 AT 300 PSIA	-200	No growth in 23,562 cycles at 20 CPM
		Termination	0.032	0.312	0.103				0.030	0.508	15.4					
WC-17	0.063	Initiation	0.027	0.287	0.094	44.7	0.22	0.10	0.025	0.429	13.8	16.2	1.92	LH_2	-423	Grew through-the-thickness in 10,950 cycles at 60 CPM
		Termination	0.063	0.287	0.220				0.046	1.0	18.7					

△ ALL SPECIMENS 2.5" WIDE

Table XV: LACK-OF-PENETRATION STATIC TESTS OF 5Al-2.5 Sn (ELI) TITANIUM WELDMENTS WITH INTERRUPTED WELDS TESTED AT 70°F IN AIR

SPECIMEN NUMBER	THICKNESS, t (Inch)	WIDTH, w (Inch)	APPARENT INITIAL FLAW DEPTH, a_i (Inch)	APPARENT INITIAL FLAW LENGTH, $2c_i$ (Inch)	APPARENT $(a/2c)_i$	GROSS STRESS AT FLAW BREAK THROUGH, σ_T (Ksi)	GROSS STRESS AT FAILURE, σ_F (Ksi)	YIELD STRENGTH, σ_{ys} (Ksi)	σ_T / σ_{ys}	σ_F / σ_{ys}	a_i / t	
1	0.059	11.80	0.008	3.150	0.0025	112.6	113.8	105.0	1.072	1.083	0.1356	1, 2
2	0.062	11.96	0.055	2.920	0.0188	22.6	65.4		0.215	0.623	0.887	3
3	0.062	11.84	0.038	3.030	0.0125	122.1	122.1		1.163	1.163	0.613	2, 3
4	0.059	11.91	0.038	2.920	0.0130	117.7	117.7	105.0	1.121	1.121	0.645	2, 3

1. SEAL PASS INCLUDED IN WELDING SEQUENCE
2. LARGE AMOUNTS OF DIFFUSION BONDING CAUSED FAILURES NEAR ULTIMATE TENSILE STRENGTH. DATA POINTS NOT INCLUDED IN PLOTS
3. SEAL PASS EXCLUDED FROM WELDING SEQUENCE

Table XVI: LACK-OF-PENETRATION STATIC TESTS OF 5Al-2.5 Sn (ELI) TITANIUM WELDMENTS WITH EDM FLAWS TESTED AT 70°F

SPECIMEN NUMBER	THICKNESS, t (Inch)	WIDTH, w (Inch)	INITIAL FLAW DEPTH, a_i (Inch)	INITIAL FLAW LENGTH, $2c_i$ (Inch)	$(a/2c)_i$	GROSS STRESS AT FLAW BREAK THROUGH, σ_T (Ksi)	GROSS STRESS AT FAILURE, σ_F (Ksi)	YIELD STRENGTH, σ_{ys} (Ksi)	σ_T/σ_{ys}	σ_F/σ_{ys}	a_i/t	ENVIRONMENT
5	0.061	11.95	0.048	2.980	0.0161	35.1	72.4	105.0	0.333	0.690	0.787	AIR
6	0.065	11.86	0.054	1.475	0.0369	42.2	N/A		0.402	N/A	0.832	AIR
7	0.062	11.89	0.037	2.468	0.0148	46.5	N/A		0.443	N/A	0.597	AIR
8	0.065	11.86	0.027	2.950	0.0092	84.2	N/A		0.802	N/A	0.416	AIR
S6	0.068	11.87	0.047	1.500	0.0313	43.6	N/A	105.0	0.415	N/A	0.694	GH_2 AT 300 PSI

Table XVII: LACK-OF-PENETRATION SUSTAINED TESTS OF 5Al-2.5 Sn (ELI) TITANIUM WELDMENTS WITH EDM FLAWS TESTED AT 70°F IN GH_2 AT 300 PSIA

SPECIMEN NUMBER	THICKNESS, t (Inch)	WIDTH, w (Inch)	INITIAL FLAW DEPTH, a_i (Inch)	INITIAL FLAW LENGTH, $2c_i$ (Inch)	$(a/2c)_i$	APPLIED GROSS STRESS, σ_A (Ksi)	YIELD STRENGTH, σ_{ys} (Ksi)	σ_A / σ_{ys}	a_i / t	SUSTAINED TIME (hours)	OBSERVATIONS
S1	0.064	11.86	0.053	2.470	0.0215	33.0	105.0	0.314	0.829	4.5	GROWTH THROUGH THICKNESS
S2	0.064	11.88	0.040	1.430	0.0280	↓	↓	↓	0.625	19.5	GROWTH (Δa = 0.006")
S5	0.062	11.87	0.032	2.920	0.0110	33.0	105.0	0.314	0.517	16.0	GROWTH (Δa = 0.010")

Table XVIII: LACK-OF-PENETRATION LOAD/UNLOAD TEST OF 5Al-2.5 Sn (ELI) TITANIUM WELDMENT WITH EDM FLAW TESTED AT 70°F IN AIR

L/U 1	0.064	11.93	0.036	2.950	0.0122	33.0	105.0	0.314	0.563	—	NO GROWTH

Table XIX: LACK-OF-PENETRATION SUSTAINED TESTS OF 5Al-2.5 Sn (ELI) TITANIUM WELDMENTS WITH EDM FLAWS TESTED AT -200°F IN GH_2 AT 300 PSIA

SPECIMEN NUMBER	THICKNESS, t (Inch)	WIDTH, w (Inch)	INITIAL FLAW DEPTH, a_i (Inch)	INITIAL FLAW LENGTH, $2c_i$ (Inch)	$(a/2c)_i$	APPLIED GROSS STRESS, σ_A (Ksi)	YIELD STRENGTH, σ_{ys} (Ksi)	σ_A / σ_{ys}	a_i / t	SUSTAINED TIME (hours)	OBSERVATIONS
S3	0.065	11.80	0.038	2.980	0.0128	33.0	145.8	0.226	0.585	20.0	GROWTH ($\Delta a = 0.010''$)
S4	0.066	11.92	0.048	1.515	0.0317	↓	↓	↓	0.727	16.0	NO GROWTH
S7	0.064	11.90	0.031	2.945	0.0105	33.0	145.8	0.226	0.485	16.0	▽ GROWTH ($\Delta a = 0.014''$)

▽ SPECIMEN PROOF TESTED IN GH_2 TO 45 KSI AT 70°F, THEN SUSTAIN LOADED TO 33 KSI AT -200°F

DISTRIBUTION LIST FOR FINAL REPORT NASA CR-114859

Contract NAS 9-11435

"CRACK GROWTH OF 5Al-2.5Sn TITANIUM IN HYDROGEN"

The Boeing Company
Seattle, Washington

National Aeronautics and Space Administration
Manned Spacecraft Center
Houston, Texas 77058

Attention:	R&D Procurement Branch M. Ballas Mail Code JC-73	1
	Technical Library Branch Retha Shirkey Mail Code BM6	1
	Management Services Division J. T. Wheeler Mail Code BM7	1
	Materials Technology Branch S. V. Glorioso Mail Code ES5	65

National Aeronautics and Space Administration
Ames Research Center
Moffett Field, California 94035

Attention:	C. Hermack	1

DMIC/DCASO
Battelle Memorial Institute
505 King Avenue
Columbus, Ohio 43201 — 2

North American Aviation, Inc.
Space and Information Systems Division
12214 Lakewood Boulevard
Downey, California 90242

Attention:	Technical Information Center D/096-722 (AJ01)	1
	L. J. Korb	1
	J. E. Collipriest	1

Grumman Aircraft Engineering Corp.
Bethpage, Long Island, New York 11714

Attention:	G. Hendry	1